Reply anonymous reviewer #1

The publication under consideration introduces a new portable spectrometer commercially available from Bruker, which offers moderate spectral resolution (max optical path difference 4.42 cm) and wide spectral coverage (680 – 5200 cm^{-1}). The authors present the instrumental setup, the methods applied for achieving radiometric calibration, and finally present a theoretical study on the presumed instrumental capabilities.
The topics addressed by the paper match well with the scope of AMT. However, in my impression, the actual elaboration falls short with respect to the premises stated in the title, so major extensions (and a readjustment of the title?) are required before the work can be considered for publication in AMTD.
The title phrase "Instrumental characteristics" would suggest that real world instrumental characteristics are elaborated and reported, what currently is reported hardly reaches beyond the specifications provided by the manufacturer.

We thank the anonymous reviewer for his careful reading of our manuscript and his many insightful comments and suggestions. After careful consideration, we are providing a revised manuscript that benefits from further calculation results, figures and rewriting of certain sections that will be discussed in details in the following answers. This revised manuscript reflects the recommendations of the reviewer, and it benefits from a slightly modified title, as suggested by the reviewer: **Instrumental characteristics and potential Greenhouse gases measurement capabilities of the Compact High-spectral Resolution Infrared Spectrometer: CHRIS**. Due to these modifications, we have considerably improved the manuscript.

First, we want to point out again that CHRIS is an instrumental prototype, and that the first part of the manuscript is dedicated to the characterization of its main characteristics that have not been provided by the manufacturer. Secondly, the potential capabilities to measure greenhouse gases are presented in the second part of the manuscript through an exhaustive information content study and a comparison with two other commercial FTIR: the EM27/SUN and the IFS125HR.

Below we respond to the questions and comments of the reviewer in detail, with reviewer comments in a different color.

1- Which SNR is achieved in the measured spectrum as function of wave number (this also requires the specification of scan speed and total scan time applied, which is not reported in the current version of the draft)?

During the acquisition of a spectrum, the amount of the signal received by the detector depends on the aperture stop diameter, which can be manually modified when the instrument is open. Since this manipulation is not easy during measurements campaigns outside the laboratory, we performed several tests in different conditions and we found that an aperture stop of 5 mm is the best compromise between a good signal and the saturation of the detector. We adopted this diameter for all the spectra recorded by CHRIS.

Furthermore, several tests allowed us the quantifying of the Signal-to-Noise Ratio (SNR) improvement with the scan number (if we increase the number of scans, we get a higher SNR, as can be shown in **Fig. 1**). However, we can see that there is no

apparent improvement between the spectra of 100 and 200 scans, and this is why we limited our number of scans to 100 for measuring CO_2 and CH_4. Moreover, the time needed for 1 scan with a scanning velocity of 120 KHz is 0.83s, so 100 scans take approximately 83s which is low in comparison with the variability of CO_2 and CH_4 in the atmosphere.

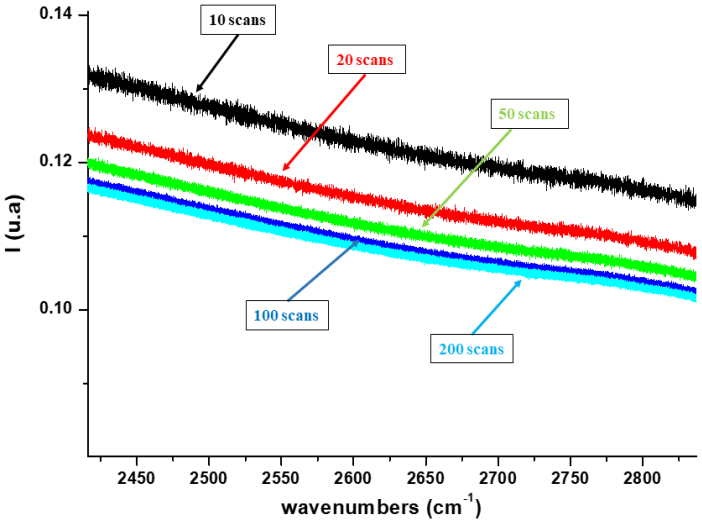

Figure 1: Improvement of the SNR with different scan number and a scan speed of 120 KHz

A typical example of the SNR of such a protocol (aperture stop diameter= 5 mm, scan speed=120 KHz and scan number=100) is shown in **Fig. 2**. The SNR varies between 20 and 845 in the covered spectral domain.

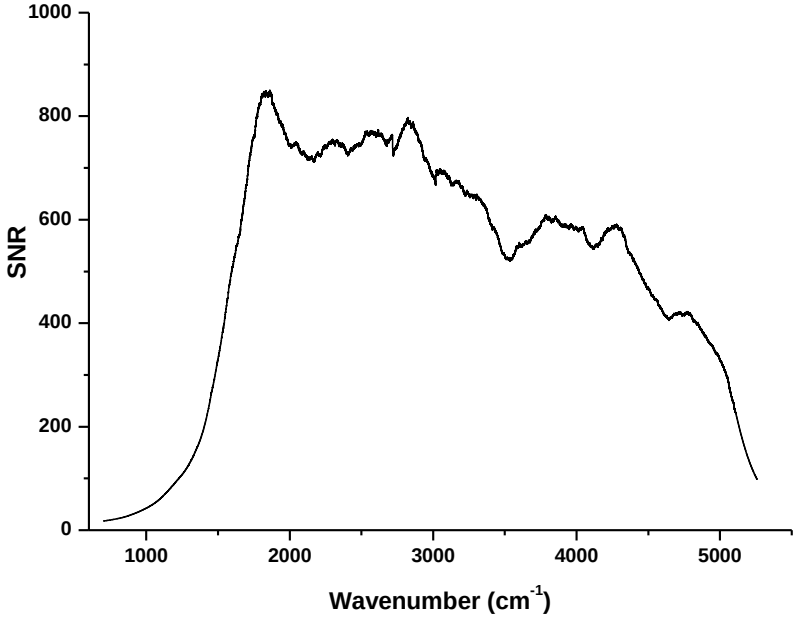

Figure 2: The SNR in function of the wavenumber for CHRIS.

These information and the figures have been added to the revised manuscript.

2- How stable are the radiometric characteristics of the device (use e.g. Allan deviation plots of spectral or derived quantities, see e.g. the investigation performed on a portable spectrometer by Chen et al., 2016)? Characterize the instrumental line shape (ILS) by using lasers, gas cells or open path measurements (see, e.g. Frey et al., 2015). Is the ILS near the nominal expectation? Does the spectrometer achieve the nominal resolution at all?

The cavity blackbody used is an HGH/RCN1250N2 certified by the LNE (Laboratoire National de métrologie et d'Essais) as having an emissivity greater than 0.99 in the spectral covered domain of CHRIS, a stability of 0.1° K at 1173° K, an opening diameter up to 50 mm (corresponding to that of CHRIS), and covering temperatures from 323 to 1523° K. This cavity blackbody is mounted on an optical bench and used before and after each campaign to perform absolute radiometric calibrations through open path measurements and make sure that this calibration is stable across the spectral range covered.

Furthermore, during campaigns and after long transportations, constant measurements of the internal blackbody, which can be heated up to 353° K, is carried out in the thermal infrared region that is the most affected by any drift. **Figure 3** shows the variations of the internal blackbody during multiple field campaigns: we can see a little fluctuation in function of the measurement conditions, but we can clearly see that depending on the locations and even years, no systematic drift can be detected, so we can safely say that the instrument is quite stable between each laboratory calibration. We give more details in the revised manuscript.

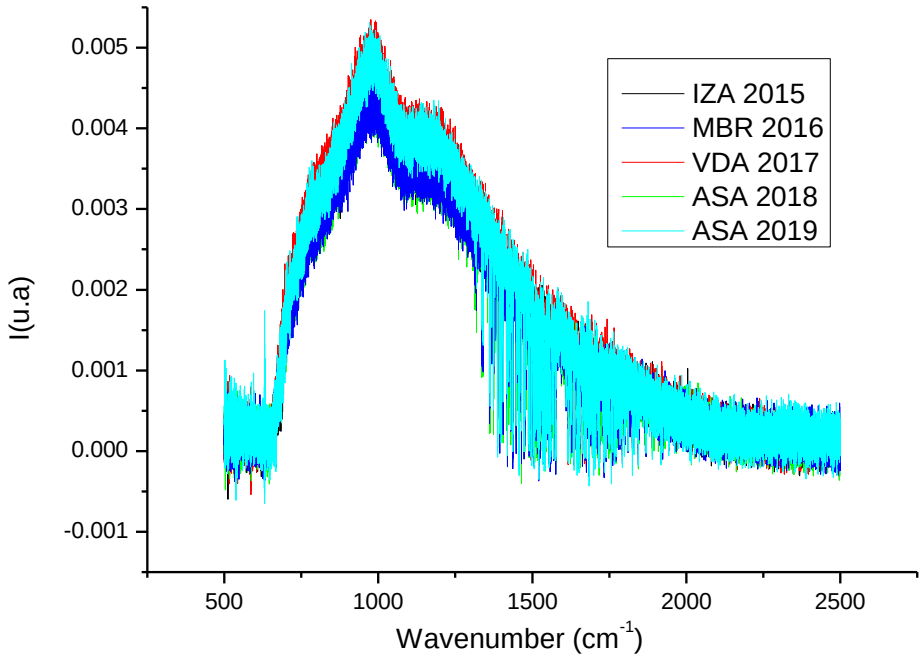

Figure 3: The radiometric stability of the instrument is achieved by following the variations of the internal blackbody during multiple field campaigns. IZA : Izana, MBR : M'Bour, VDA : Villeneuve d'Ascq, ASA : Aire-sur-l'Adour.

Since CHRIS is a prototype, there is no nominal expectation other than having a resolution at least similar or better than the future satellite sounders, e.g. IASI-NG (0.25 cm^{-1}). The tests conducted by the manufacturer confirmed that the spectral resolution is better than 0.2 cm^{-1}, which matches the original request.

Regarding the ILS, no information was provided upon delivery of the instrument, and since we were not equipped with the proper tools, there was no detailed information dedicated to the characterization of the ILS. Nevertheless, with the help of colleagues from the PC2A laboratory, we performed one open path ILS measurement alongside the pre-spectral calibration by using our cavity blackbody as source as it is previously done in Wiacek et al. 2007. We recorded the spectrum without applying any apodization, and with the help of the radiative transfer algorithm, ARAHMIS, developed at our laboratory we determined the ILS corresponding to a MOPD of 4.42 cm and a spectral resolution of 0.135 cm^{-1} using a sinc function, which matches our expectations.

However, in order to characterize the ILS more regularly, we are in the process of modifying our laboratory optical bench to include gas cell measurements before the next field campaign which will take place this summer. Note that the ILS parameters can be easily modified in our RT code ARAHMIS, during the retrieval process.

3- On which levels other well-known important kinds of spectral artefacts are controlled which might critically detoriate retrieval quality? For a broadband spectrometer covering more than one octave along the frequency axis non-linearity, double passing and sampling ghosts need to be investigated.

The following information have been added to the revised manuscript:

There are commonly several well-known spectral artifacts: the aliasing, the picket-fence effect also known as the resolution bias error, and the phase correction, which are controlled in CHRIS. Several tests were performed on this instrument to investigate its optical and technical properties and the results are presented below.

An aliasing is the result of the missampling of the interferogram in the x-axis locations, which leads to errors in the retrieved column abundances due to its overlap with the original spectrum. Sampling positions are derived from the zero crossings of a He-Ne laser wave having a wavenumber of 15800 cm^{-1}. As a zero crossing occurs every $\lambda/2$, the minimum possible sample spacing is Δx=1/31600 cm. This corresponds to a folding wavenumber ($\nu_f = 1/(2.\Delta x)$) of 15800 cm^{-1}, i.e. the maximum bandwidth that can be measured without overlap has a width of 15800 cm^{-1}. This source error is of special relevance to the spectra acquired in the NIR region. However, for the MIR, the investigated bandwidth is much smaller than 15800 cm^{-1}, where ν_{max} is less than 5200 cm^{-1} for CHRIS's spectra so they are not affected by this problem (Dohe et al. 2013).

The picket-fence effect, or the resolution bias error, becomes evident when the interferogram contains frequencies, which do not coincide with the frequency sample points, but this is overcome in our spectra by the classical method of the Zero Filling Factor (ZFF) where the number of points is doubled in the original interferogram.

The phase correction is necessary while converting the interferogram into a spectrum, which is relevant to single-sided measurements, similar to those acquired by CHRIS since its interferometer cannot operate in a double-sided mode. Mertz phase correction is the method used in CHRIS to overcome this problem.

During our tests, we noticed that when using a scan speed of 160 KHz, we drastically increase the non-linearity effect of the detector (**Fig. 4**). However, we identified a ghost signal for low scanning velocities (for example 40 KHz shown in **Fig. 5**). This ghost is specific to CHRIS because it is caused by the noise introduced from the vibrations of the compressor used in the closed-cycle stirling cooler. The choice of a scanning velocity of 120 KHz is a compromise between two important features: the elimination of the ghost signal, which appears at scanner velocities below 80 KHz, and the increase of the detector non-linearity at a velocity of 160 KHz.

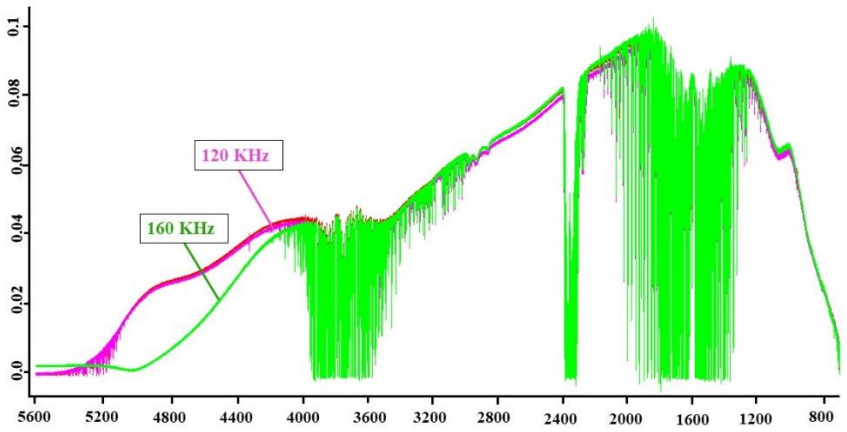

Figure 4: Spectra of the external cavity blackbody with two different scanning velocities.

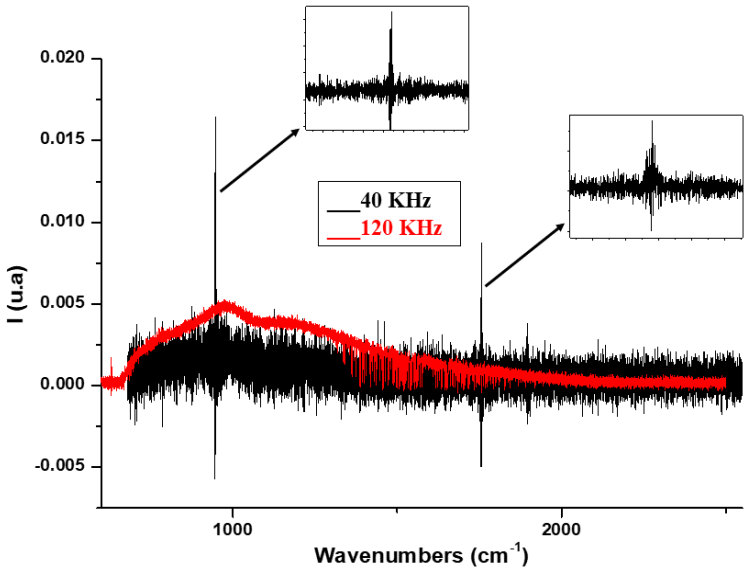

Figure 5: Spectra of the internal blackbody of CHRIS with a scanner velocity of 40 KHz.

4- The spectrometer offers higher spectral resolution than other portable units described earlier by other investigators. Nevertheless, it still uses a similar non-stabilized He-Ne laser (which might drift during recording interferograms). Which recommendations concerning applied scan speed result from this? How many interferograms can be coadded before spectral recalibration is needed in order to avoid degradation of spectral resolution?

As said before (see answer 1), several tests were performed to find the best compromise of the above-mentioned parameters to achieve good spectral quality. For the covered spectral domain, one recorded interferogram consists of 99527 points with a scanner velocity of 120 KHz, which corresponds to a scan time of 0.83 s. The protocol was chosen in a way that when co-adding 100 interferograms, the total time required to measure a spectrum is 83 s, which is low in comparison with the variability of these gases in the atmosphere, so spectral degradation is avoided. Furthermore, the spectral parameters are adjustable at each inversion and for each spectrum in the RT model ARAHMIS.

The title phrase “Greenhouse gases measurement capabilities” would suggest that some kind of empirical validation and verification with respect to other independent observation systems is performed. A high level of precision and accuracy needs to be achieved (in the sub percent range), otherwise remotely-sensed measurements of column-averaged abundances of carbon dioxide or methane are essentially useless due to the low variability of these long-lived gases in the atmosphere. The TCCON was the first network to solve this task for ground based solar absorption spectroscopic observations. The successful strategy was to extend spectral observations into the near infrared including the 1.26 um band of molecular oxygen, so transferring the absolute measurement of a column amount into a relative measurement of the ratio of the target gas column to the column of molecular oxygen. Target gas and oxygen column amounts are derived from the same spectrum and the fact that the dry molar fraction of molecular oxygen is well known can be exploited. This strategy reduces the impact of many instrumental and other detrimental effects. It is difficult to see how a spectrometer not using the oxygen reference can match the abovementioned requirements. For demonstrating that the quality of data collected with CHRIS nevertheless is sufficient for validation and other purposes, a long-term side-by-side empirical test next to a TCCON spectrometer would be required. The period of investigation should cover at least one year for demonstrating the measurements can reproduce the annual cycle of the column-averaged abundances and for investigating possible biases related to atmospheric humidity, solar elevation, and other possible impact factors. Stability characteristics of the portable EM27/SUN spectrometer have been investigated by Frey et al., 2018 (measuring three years side-by-side to a TCCON spectrometer). First results of a long-term study performed at the TCCON site Sodankyla encompassing different kinds of portable spectrometers have recently been presented by Sha et al. (currently handled in AMTD: AMT-2019-371).

Indeed, we agree that measuring the oxygen column allows the determination of the carbon dioxide column where systematic effects are eliminated (Wunch et al.

2011). However, there is another option for calculating the column-averaged dry mole fraction without using the oxygen reference. Based on the formula given in Wunch et al. (2010) and used in Zhou et al. (2018), we can calculate X_G for CO_2 and CH_4:

$$X_G = \frac{column_G}{column\ dry\ air}$$

$$column\ dry\ air = \frac{P_s}{\{g\}_{air} m_{air}^{dry}} - column_{H_2O} \frac{m_{H_2O}}{m_{air}^{dry}}$$

Where m_{H_2O} and m_{air}^{dry} are the mean molecular masses of water and dry air, respectively, P_s is the surface pressure and $\{g\}_{air}$ is the column-averaged gravitational acceleration. Therefore, the calculation of X_G is possible if all these parameters are available, particularly in the MAGIC framework where we have access, along with all the instruments involved, to the balloons and radiosondes data (temperature, surface, pressure, H_2O vmr, etc…). However, the two equations for the calculation of X_G are not strictly similar since the EM27/SUN eliminates the systematic errors that are common to the target gas and O_2 column retrievals. Addressing this issue, this paragraph is rewritten in the revised manuscript to eliminate any ambiguity.

We would like to mention that during MAGIC, CHRIS also performed simultaneous measurements co-located spatially and temporally with the EM27/SUN and the IFS125HR of the TCCON network, and the retrieval process and the calculation of X_G using ARAHMIS is the subject of the study that had just begun and will be presented in an upcoming paper.

Judging from these studies and the experiences gained by TCCON, main obstacles in achieving the desired quality level are all kinds of practical instrumental issues and various details of the data processing, which all need to be addressed. The argumentative connection between the schematic theoretical information content analysis presented by the authors and the actual "greenhouse gases measurement capabilities" of CHRIS therefore seems weak. The theoretical study can only provide a rather optimistic theoretical extrapolation of the instrument's capabilities, and would suggest a modified title as "…and potential Greenhouse gases measurement capabilities …" or alike.

We agree that we do not present direct measurement capabilities of CO_2 and CH_4, so the main objective of this study is to investigate the potential capabilities of this instrumental prototype to measure greenhouse gases, hence the adjustment of the title as suggested by the reviewer. Nevertheless, in order to have results that are more reliable, we added to the revised manuscript the same information content study but using covariance matrices taken from TCCON data and close to those determined in Eguchi et al. 2010.

I would recommend adding substantial empirical evidence concerning the capabilities of measuring greenhouse gases, especially as the spectrometer was already operated side-by-side to a TCCON spectrometer on Tenerife island and I assume together with other instruments and aircore soundings during MAGIC. I understand that the data analysis scheme for CHRIS is still under development, but well-characterized codes for the processing as GFIT are available and could be used meanwhile.

Indeed, as mentioned before this substantial empirical evidence of the real capacities of the instrument is the main objective of the work that had just begun, within the framework of MAGIC, on the retrieval process of CHRIS. The latter is processed alongside different types of instrument: the ground-based commercial instruments like the IFS125HR from TCCON and the EM27/SUN; but also the methane lidar, the Aircore and the Amulse, and will therefore be the subject of the upcoming paper. We will use for these retrievals the radiative transfer model ARAHMIS, which has the particularity to apply the retrieval of absolute radiances on different spectral regions simultaneously, including the thermal band.

5- Under Equation 5 it is stated that the forward model F takes into account surface emissivity – not a good example in case of an upward looking solar absorption spectrometer as considered here:

Surface emissivity is not considered in the forward model F. It is a mistake which is corrected in the revised manuscript.

6- Line 235: the model atmosphere extends only up to 20 km altitude? This neglects a non-negligible fraction of the total column for e.g. carbon dioxide:

The DOFS of CO_2 at a zenithal angle of 10° at 40 km is 3.54 compared to 3.49 at 20 km, which shows that we have a weak sensitivity above 20 km. Furthermore, the profiles acquired by the instruments on-board the planes and balloons during MAGIC extend to 25 km, so we took into consideration the reviewer advice and we extended our study to 40 km to match the altitudes reached by TCCON as seen in **Figure 6**. All the new DOFS and figures are corrected accordingly in the revised manuscript.

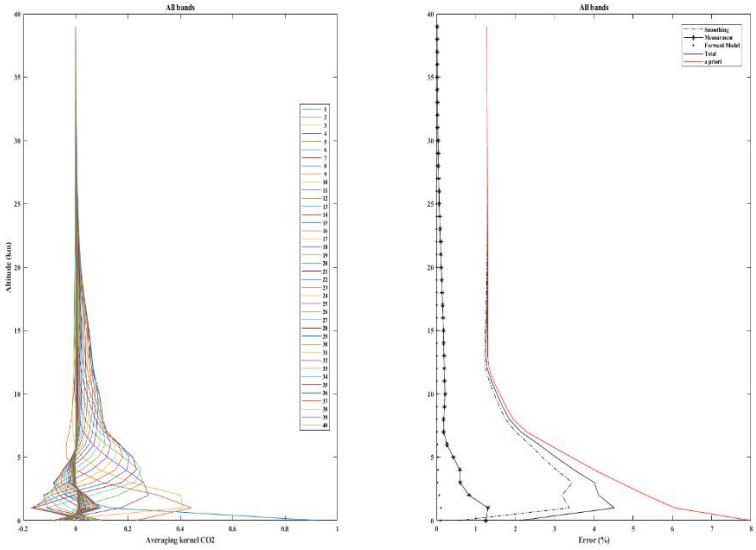

Figure 6: The averaging kernel for CO_2 of CHRIS from 0 to 40 km in altitude.

7- Line 240: The assumption of zero off-diagonal elements in the a-priori covariance for long-lived greenhouse gases is highly unrealistic. Climatological data describing the variability of greenhouse gases profiles are available and should be used.

One of the main objectives of the acquisition of CHRIS is the validation of the space instruments, like TANSO-fts/ GOSAT, which has similar spectral bands. In a previous study (Herbin et al. 2013), diagonal a-priori covariance matrices were used, so for the sake of comparison we used the same matrices. Moreover, the use of diagonal a-priori covariance matrices is common for the retrievals from space measurements (e.g. De Wachter et al. 2017).

However, in our retrieval process we will use the more realistic a priori covariance matrix mentioned before. In the revised paper, the study with the two matrices is shown.

8- Line 255: Handling water vapor as a non-retrieved parameter does not match with retrieval strategies as applied in practice. Water vapor will be part of the retrieved state vector if in the spectral range under consideration it is not negligible as interfering species:

As mentioned before, since this information content study has to be easily compared to measurements from space instruments, we considered variability for the water vapor profile as derived from the IASI level 2 products provided by EUMETSAT (Herbin et al. 2013, De Wachter et al. 2017). However, we agree that the impact of water is very important, and in the work that had just begun on the CO_2 retrieval, H_2O is part of the retrieved state vector. This information is mentioned in the revised manuscript.

9- Table 2 is inconsistent. Either "IFS125HR" refers to a TCCON spectrometer, then 45 cm MOPD is correct or it refers to an IFS125HR spectrometer operated by NDACC, in this case the 0.005 cm^{-1} resolution is reasonable. The specified spectral range is incorrect for either network. From the viewpoint of an information content analysis it might be preferable to separate the two kinds of spectrometers, the FTIR spectrometers operated in the framework of NDACC and those operated by TCCON.

The information content analysis in the revised manuscript takes into consideration the characteristics of the two networks and therefore we separated our study to respect the characteristics of each network.

10- Line 325: Both TCCON and EM27/SUN (dual-channel version) spectrometers offer a lower wavenumber limit of about 4000 cm^{-1}:

We agree that this sentence is unclear, therefore in the revised manuscript it is replaced by the following: "… the TCCON network begin their measurements at 4000 cm^{-1} that allowed us the comparison with the band 3 of CHRIS (for both CO_2 and CH_4). However, the EM27/SUN have no exploitable signal before 4700 cm^{-1} (Gisi et al. 2012), therefore the CH_4 absorption lines do not show in the common band between CHRIS and the EM27/SUN…"

The following references have been added to the revised manuscript:

Wiacek, A., Taylor, J. R., Strong, K., Saari, R., Kerzenmacher, T. E., Jones, N. B., Griffith, D. W. T.: Ground-Based Solar Absorption FTIR Spectroscopy: Characterization of Retrievals and First Results from a Novel Optical Design Instrument at a New NDACC Complementary Station, Journal of Atmospheric and Oceanic Technology, 10.1175/JTECH1962.1.

Dohe, S., Sherlock, V., Hase, F., Gisi, M., Robinson, J., Sepúlveda, E., Schneider, M., and Blumenstock, T.: A method to correct sampling ghosts in historic near-infrared Fourier transform spectrometer (FTS) measurements, Atmos. Meas. Tech., 6, 1981–1992, https://doi.org/10.5194/amt-6-1981-2013, 2013.

Eguchi, N., Saito, R., Saeki, T., Nakatsuka, Y., Belikov, D., and Maksyutov, S.: A priori covariance estimation for CO_2 and CH_4 retrievals, J. Geophys. Res., 115, D10215, doi: 10.1029/2009JD013269, 2010.

De Wachter, E., Kumps, N., Vandaele, A. C., Langerock, B., and De Mazière, M.: Retrieval and validation of MetOp/IASI methane, Atmos. Meas. Tech., 10, 4623–4638, https://doi.org/10.5194/amt-10-4623-2017, 2017.

Reply anonymous reviewer #2

The paper introduces a new portable Fourier Transform Spectrometer (FTS) with a higher resolution than other commercially available portable FTS instruments. The characteristics of the instruments are described in detail and methods for spectral and radiometric calibration are implemented. The information content to retrieve the vertical profile information of CO_2 and CH_4 and the associated errors are explained and compared to two other FTS instruments that are widely used within the remote sensing community. The optimized number of channels to retrieve CO_2 and CH_4 are carried out at the end.
The work presented in the manuscript is within the scope of AMT. The text sometimes becomes unclear and hard to follow. I suggest reviewing the transitions between topics and fleshing out when a new topic is introduced to make it easier for the readers to follow along.

We thank the anonymous reviewer for his careful reading of our manuscript. After thorough consideration, we are providing an improved manuscript that reflects his insightful suggestions and comments with a slightly modified title as follows: **Instrumental characteristics and potential Greenhouse gases measurement capabilities of the Compact High-spectral Resolution Infrared Spectrometer: CHRIS.** As recommended, this revised manuscript benefits from clearer transitions between topics and rewriting some of sentences/sections, as well as further calculation results and figures that will be discussed in details in the following answers.

Below we respond to the questions and comments of the reviewer in detail, with reviewer comments in a different color.

1- The MAGIC campaign has been brought up a few times in the manuscript, however, it's unclear when exactly that campaign took place? How many days of measurement are available from each instrument involved?

The MAGIC campaigns are annual campaigns held at different locations in France (see **Fig. 1**), with the collaboration of different French laboratories: LMD, GSMA, LERMA, LSCE, and the LOA. In the future, these campaigns will be organized once or twice a year: once in France and once at the stratospheric balloon release sites (Kiruna, Sweden and Timmins, Canada). Up until now, there are about ten days of data available for each instrument involved during the last two campaigns. The objective is the monitoring of the emission of GHG, mainly CO_2 and CH_4, and to provide regular mobile data for the validation of the current and future space missions, like Merlin, Microcarb and IASI-NG.

We want to point out again that CHRIS is an instrumental prototype, and that MAGIC offers the ideal framework to its characterization, which motivated the first part of the manuscript. The potential capabilities to measure greenhouse gases are presented in the second part of the manuscript through an exhaustive information content study and a comparison with two other commercial FTIR: the EM27/SUN and the IFS125HR. However, the context of these campaigns and the scientific analysis of the measurements made by CHRIS and the inter-comparisons with the different instruments involved, will be detailed in an upcoming paper. Some extra details on MAGIC are mentioned in the revised manuscript.

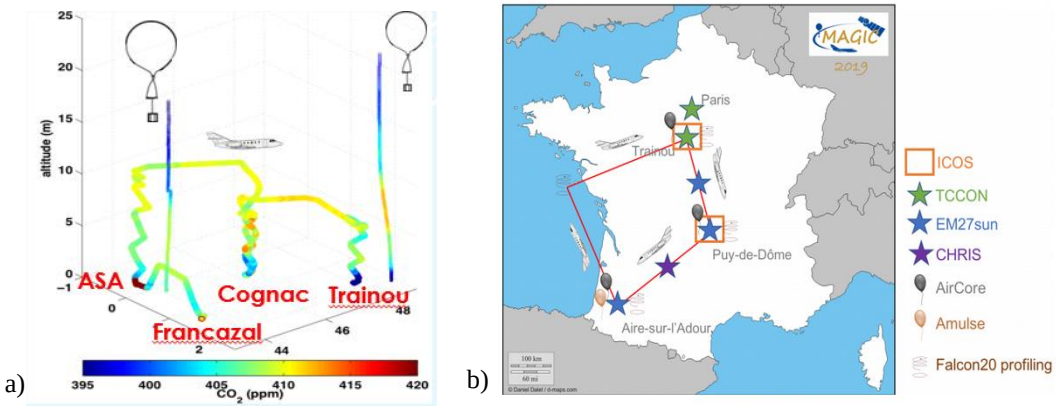

Fig 1: CO_2 vertical concentration and instrument deployment for the MAGIC campaigns: a) 2018 and b) 2019

2- The title of the manuscript suggests "greenhouse gas measurement capabilities" of the instrument are discussed in the paper. However, the main focus of the paper is on the information that could be obtained for the vertical profiles of CO_2 and CH_4 and there's no presentation of retrieved column values. Given that two other instruments (125-HR and EM27/SUN) were measuring at the same time as CHRIS, comparison of CO_2 and CH_4 column values between the three instruments could be proving the "greenhouse gas measurement capabilities" of CHRIS. GGG could easily be used perform the retrievals.

Indeed, we agree that the objective of this paper is the investigation of the potential capabilities of this instrument to measure the greenhouse gases, hence the adjustment of the title. The real capacities of this instrument and the preliminary results of the retrieval process is the main objective of the work that had just begun on CHRIS, within the framework of MAGIC. The latter is processed alongside different types of instruments: the ground-based commercial instruments like the IFS125HR from TCCON and the EM27/SUN; but also a methane lidar, the Aircore and the Amulse, and will therefore be the subject of the upcoming paper. However, we will use for these retrievals the radiative transfer model ARAHMIS, which has the particularity to apply the retrieval of absolute radiances on different spectral regions simultaneously, including the thermal band.

3- In section, 2.2.1 it is mentioned that 50, 100 spectra are coadded for CO_2 and CH_4 measurements. My calculations using the laser frequency and scanner velocity suggests a single scan time of about 0.7 s. Can you confirm this number? If that's the case, caoadding 100 spectra is still fast enough not to worry about changes in the atmosphere and also stability of the laser.

Indeed, for the covered spectral domain, one recorded interferogram consists of 99527 points with a scanner velocity of 120 KHz, which corresponds to a scan time of 0.83 s. After several tests on the scan velocity and the scan number, we found that the best compromise to measure CO_2 and CH_4 is a scan speed of 120 KHz and a scan number of 100. With this protocol, the total time required to record a spectrum is 83 s, which is low in comparison to the variability of these gases in the atmosphere. Furthermore, a scan velocity of 120 KHz was chosen as a compromise between two important features: the elimination of the ghost signal, which appears at scan velocities below 80 KHz that result from the vibrations of the compressor of

the closed-cycle stirling cooler, and the increase of the detector non-linearity at a velocity of 160 KHz. Note that the spectral parameters are adjustable at each retrieval and for each spectrum in the radiative transfer model ARAHMIS.

4- Although H_2O absorption lines are present in almost all spectral windows, water vapour mole fractions are not retrieved in the analysis. Is it because of the certain meteorological conditions in Izaña that leads to stable water vapour values? Bringing some evidence to prove that's the case would be helpful.

One of the main objectives of the acquisition of CHRIS is the validation of the space instruments, like TANSO-fts/ GOSAT, which has similar spectral bands. Since this information content study has to be easily compared to measurements from space instruments, we considered variability for the water vapor profile as derived from the IASI level 2 products provided by EUMETSAT (Herbin et al. 2013, De Wachter et al. 2017). However, we agree that the impact of water is huge, and in the work that had just begun on the CO_2 retrieval, H_2O is part of the retrieved state vector. This information is mentioned in the revised manuscript.

5- In section 3.1, it is mentioned the apriori profiles (I am guessing of CO_2 and CH_4), temperature and humidity are used for the analysis. Could you please specify where these information are obtained from?

During campaigns, the a priori profiles for the temperature, pressure and water vapor are derived from the radiosondes located both spatially and temporally near our instrument. Otherwise, we take, when available, the radiosondes data located as close as possible to our measurement point. The CO_2 and CH_4 a priori profiles are interpolated from the available satellite instruments Level 2 profiles and/or NDACC/TCCON a priori profiles.

6- Page 13, the last paragraph, you mention that calculation of X_G using O_2 column values done by EM27/SUNs allows comparisons with satellite data and it's not possible for CHRIS. This statement contradicts the point made earlier in the introduction where you suggest CHRIS could be used for satellite validation. In fact, retrieval of X_G values are possible for CHRIS if surface pressure and water vapour measurements are used as described by Wunch et al., 2010.

Indeed, this part of the manuscript might be confusing, and we agree that the retrieval of X_G values is possible for CHRIS if the formula in Wunch et al. 2010 is used. During the MAGIC campaigns, we have access to the balloons and radiosondes data (temperature, surface pressure, H_2O vmr, etc…); so for these particular campaigns, X_G values will be calculated for CHRIS and the results will be compared with the other instruments involved, especially the IFS125HR of the TCCON network and the EM27/SUN, and this will be the subject of the upcoming paper. However, what we want to point out is the fact that the two equations to calculate X_G are not strictly similar since the EM27/SUN can measure O_2 column to calculate the DMFs, which eliminates the systematic errors due to the measurements which will not be possible for us, since the O_2 band is not detected by CHRIS. This paragraph is rewritten in the revised manuscript to eliminate any ambiguity.

Manuscript prepared for J. Name
with version 5.0 of the LaTeX class copernicus.cls.
Date: 5 April 2020

Instrumental characteristics and potential Greenhouse gases measurement capabilities of the Compact High-spectral Resolution Infrared Spectrometer: CHRIS.

Marie-Thérèse El Kattar[1], **Frédérique Auriol**[1], **and Hervé Herbin**[1]

[1]Univ. Lille, CNRS, UMR 8518 - LOA - Laboratoire d'Optique Atmosphérique, F-59000 Lille, France

Correspondence to: Hervé Herbin
(herve.herbin@univ-lille.fr)

Abstract. Ground-based high spectral resolution infrared measurements are an efficient way to obtain accurate tropospheric abundances of different gaseous species and in particular GreenHouse Gases (GHG), such as CO_2 and CH_4. Many ground-based spectrometers are used in the NDACC and TCCON networks to validate the Level 2 satellite data, but their large dimensions and heavy mass makes them inadequate for field campaigns. To overcome these problems, the use of portable spectrometers was recently investigated. In this context, this paper deals with the CHRIS (Compact High-spectral Resolution Infrared Spectrometer) prototype with unique characteristics such as its high spectral resolution (0.135 cm^{-1} non-apodized) and its wide spectral range (680 to 5200 cm^{-1}). Its main objective is the characterization of gases and aerosols in the ~~infrared thermal~~ thermal and shortwave infrared region, that's why it requires high radiometric precision and accuracy, which is achieved by performing spectral and radiometric calibrations that ~~will be presented~~ are described in this paper. Also, CHRIS's capabilities to retrieve CO_2 and CH_4 vertical profiles are presented through a complete information content analysis, a channel selection and an error budget estimation in the attempt to join the ongoing campaigns, such as MAGIC (Monitoring of Atmospheric composition and Greenhouse gases through multi-Instruments Campaigns), to monitor the GHG and validate the actual and future space missions such as IASI-NG and Microcarb.

1 Introduction

Remote sensing techniques have gained a lot of popularity in the past few decades due to the increasing need of a continuous monitoring of the atmosphere (Persky (1995)). Greenhouse gases, trace gases but also clouds and aerosols are detected and retrieved, thus improving our understanding of the chemistry, physics and dynamics of the atmosphere. Global scale observations are achieved using satellites, and one major technique is the InfraRed High Spectral Resolution spectroscopy (IRHSR). This technique offers radiometrically precise observations at high spectral resolution (Revercomb et al. (1988)), where quality measurements of absorption spectra are obtained. TANSO-FTS (Suto et al. (2006)), IASI (Clerbaux et al. (2007)) and AIRS (Aumann et al. (2003)) are examples of satellite sounders covering the Thermal InfraRed (TIR) region. The observations acquired from such satellites have many advantages such as: day and night data acquisition, possibility to measure concentrations of different gases, the ability to cover the land and sea surfaces (Herbin et al. (2013a)), and the ~~advantage~~ added characteristic of being highly sensitive to ~~aerosols types~~ various types of aerosol (Clarisse et al. (2010)). These spectrometers also have some disadvantages: local observations are challenging to achieve due to the pixel size that limits the spatial resolution, and the sensitivity in the low atmospheric layers is weak, where many short-lived gaseous species are emitted but rarely detected. To fill these gaps, ground-based instruments are used as a complementary technique and one famous high-precision Fourier transform spectrometer is the IFS125HR from Bruker™, which will be briefly discussed in Section (3.5), further details can be found in Wunch et al. (2011). ~~Twenty~~ More than thirty instruments are currently deployed all over the world in two major international networks: TCCON (https://tccondata.org/) and NDACC (https://www.ndsc.ncep.noaa.gov/). This particular instrument has a very large size (1x1x3 m) and a mass well beyond a hundred kilograms, and therefore achieving a long optical path difference leading to a very high spectral resolution (0.02 and 5x$10^{-3}cm^{-1}$ for TCCON and NDACC respectively). Despite its outstanding capabilities, this spectrometer is not suitable for field campaigns so it is mainly used to validate the Level 2 satellite data, thus limiting the scientifically important ground-based extension of atmospheric measurement ~~on a global scale~~around the world.

One alternative is the new IFS125M from Bruker (Pathatoki et al. (2019)) which is the mobile version of the well-established IFS125HR spectrometer. This spectrometer provides the highest resolution available for a commercial mobile FTIR spectrometer but it still has a length of about 2 m and requires on-site realignment by qualified personnel. Another alternative is the use of several compact medium-to-low resolution instruments that are currently under investigation such as a grating spectrometer (0.16 cm^{-1}), a fiber Fabry-Perot interferometer (both setups presented in Kobayashi et al. (2010)) and the IFS66 from Bruker (0.11 cm^{-1}) described in Petri et al. (2012). The ~~EM27-SUN~~ EM27/SUN is the first instrument that offered a compact optically stable, high ~~Signal-to-noise ratio~~Signal-to-Noise Ratio (SNR), transportable spectrometer (Gisi et al. (2012)) that operates in the SWIR (Short Wavelength InfraRed) region. A new prototype called CHRIS (Compact High spectral Resolution Infrared Spectrometer) was conceived to satisfy some very specific characteristics: high spectral resolution (0.135 cm^{-1}, better than TANSO-FTS and the future IASI-NG); a large spectral band (680-5200 cm^{-1}) to cover the current and future ~~satellite~~ infrared satellite spectral range and optimize the quantity of the measured species~~that will allow us the validation of the satellite data~~. Furthermore, this prototype ~~had to be transportable and could~~ is transportable and can operate for several hours on battery ~~so it will be~~ (>12H) so it is suitable for field campaigns. The full presentation of the characteristics and the calibration of this instrumental prototype ~~will be~~ is presented in Section 2.

Since carbon dioxide (CO_2) and methane (CH_4) are the two main greenhouse gases emitted by human activities, multiple campaigns have been ~~put in place like~~ worked out such as the MAGIC (Monitoring of Atmospheric composition and

Greenhouse gases through multi-Instruments Campaigns) initiative, to better understand the vertical exchange of these GHG along the atmospheric column and to contribute to the preparation and validation of future space missions dedicated to ~~monitor GHG~~ GHG monitoring. CHRIS is part of this ongoing mission and this work ~~will demonstrate~~ presents for the first time the capabilities of such a setup in achieving GHG measurements, where the forward model, state vector and error analysis ~~will be~~ is explained in Section 3.

In this context, we present in Section 3.5, a complete information content study for the retrieval of CO_2 and CH_4 of two other ground-based instruments that also participated in the MAGIC campaign: a comparison study with the IFS125HR instrument; and since CHRIS and ~~EM27-SUN~~ EM27/SUN have a common band in the SWIR region, a study to investigate the spectral synergy in order to quantify the complementary aspects of the TIR/SWIR/NIR coupling for these two instruments. Moreover, Section 4 describes the channel selection made in this study. Finally, we ~~will~~ summarize our results and ~~present~~ perspectives for future applications; in particular, the ~~inversion of GHG~~ retrieval of GHG in the MAGIC framework.

2 The CHRIS spectrometer

CHRIS is an instrumental prototype built by Bruker™ and used in different domains of atmospheric optics where its recorded spectra contains signatures of various atmospheric constituents such as ~~gases~~ GHG (H_2O, CO_2, CH_4), and ~~other particular species~~trace gases. The capacity to measure these species from a technical point of view as well as the characterization of this prototype in terms of spectral and radiometric calibrations ~~will be~~ is presented in the following ~~sections~~subsections.

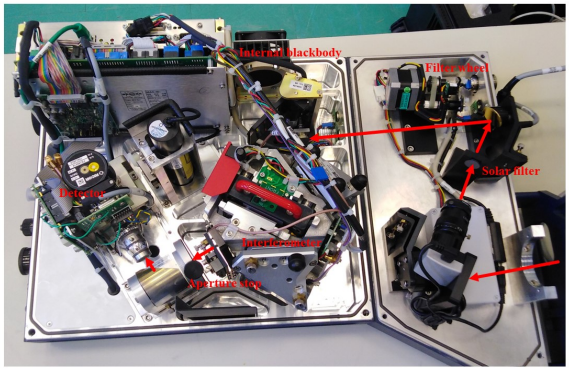

Fig. 1: An internal look of CHRIS, the red arrows illustrates the optical path of the solar beam inside the spectrometer.

2.1 General characteristics

CHRIS is a portable instrumental prototype with a mass of approximately 40 kgs and dimensions of 70x40x40 cm which makes it easy to operate on the field. The tracker, similar to the one installed on the ~~EM27-SUN~~ EM27/SUN and described in details in Gisi et al. (2012), leads the solar radiation through multiple reflections on the mirrors to a wedged fused silica window.

An internal look of CHRIS is shown in Fig. 1, where the optical path of the solar beam is represented with red arrows: after multiple reflections on the tracker's mirrors, the solar radiation enters the spectrometer through the opening and is then reflected by the first mirror where the CCD camera verifies the collimation of the beam on the second mirror having ~~the~~ a solar filter. At this level, CHRIS have a filter wheel that can be equipped with up to 5 optical filters with a diameter of 25mm. Filters are widely used when making solar measurements to reduce noise and non-linearity effects. After reflection on the second mirror, the beam enters the ~~rock solid~~ RockSolid™ Michelson interferometer which has two cube-corner mirrors to ensure the optical alignment stability of the beam and a KBr beamsplitter. After that, the radiation is blocked by an adjustable aperture stop which can be set between 1 and 18 mm. This limits the parallel beam parameter, and can be used to reduce the intensity of the incoming sunlight in case of the saturation of the detector. The remaining radiation falls on ~~the MCT~~ a MCT (Mercury Cadmium Telluride) detector, then it is digitized to obtain the solar absorption spectra in arbitrary units. This detector ~~is known for its non-linearity and~~ uses a closed-cycle stirling cooling system (a.k.a. cryo-cooler) so no liquid nitrogen has to be used. As the vibrations of the compressor may introduce noise in the spectra (see Sect. 2.6), a high scanning velocity (120 KHz) is ~~used~~needed.

A standard non-stabilized He-Ne laser controls the sampling of the interferogram. The condensation of the warm humid air on

the beamsplitter due to its transportation between cold and warm environments, is the main reason of the use of a dessicant cartridge, so the spectrometer can operate in various environmental conditions. CHRIS has also an internal blackbody, which can be heated up to 353 K to make ~~that~~ sure that there is no ~~potential~~ drift in the TIR region, and it also serves as an optical source to verify regularly the response of the detector.

2.2 Measurements and analysis

CHRIS~~has a Maximum~~ 's method of data acquisition is explained as follows: the interferograms are sampled and digitized by an Analogue-to-Digital Converter (ADC), and then numerically resampled at constant intervals of Optical Path Difference (~~MOPD) of 4.42 cm resulting in a non-apodized spectral resolution of 0.135 cm^{-1} with a spectral sampling every 0.06025 cm^{-1} to satisfy the Nyquist criterion.~~ OPD) by a He-Ne reference laser signal controlled by the aperture stop diameter. In order to determine a suitable compromise between the latter and to avoid the saturation of the signal, measurements must be done in a clear (no clouds or aerosols) and non-polluted (no gases with high chemical reactivity) atmosphere. For this purpose, a field campaign was carried out at the "El Observatorio Atmosférico de Izaña" (28.30°N, 16.48°W) in the Tenerife island. This particular observatory site is high in altitude (2374 m), away from pollution sites and has an IFS125HR listed in both the NDACC and TCCON networks. Saturation of the CHRIS's detector is reached at a value of 32000 ADC. The MCT detector is known for its high photometric accuracy but it also exhibits a non-linear response with regard to the energy flux in cases of high incident energy. This led us to choose an aperture stop of 5 mm, which is the best compromise between saturation and incoming energy flux.

Each spectrum corresponds to the solar transmission light in the total atmospheric column in a Field Of View (FOV) of 0.006 mrad. The spectral range spans the region from 680 to 5200 cm^{-1} (1.9 to 14.7 µm) which corresponds to the Middle InfraRed region (MIR). The ~~Signal-to-Noise Ratio (SNR) is an estimation of the root mean squared noise of the covered spectral domain and can be calculated in OPUS (the running program for CHRIS) using the function SNR with option fit parabola; it is estimated to be approximately 780. These instrumental qualities, summarized~~ water vapor causes the saturation we see between the bands, thus the 0 signal. Therefore, we divided the spectrum into 4 distinctive spectral bands presented in Table 3~~, will enable this prototype not only to measure CO_2 and CH_4, but also to detect other trace gases with weak absorption.~~: BT (thermal band: 680-1250 cm^{-1}), B1 (1800-2300 cm^{-1}), B2 (2400-3600 cm^{-1}) and B3 (3900-5200 cm^{-1}) and this annotation is used for the rest of the paper.

~~Representation of 3 spectra with 3 different scan number.~~

2.2.1 ~~Technical study~~

2.3 Optical features

A technical study was conducted on this prototype in order to evaluate its ~~capabilities~~optical and technical properties with a constant aperture stop diameter of 5 mm. One of the most important findings is the effect of the number of scan on the measured spectra. In practice, a scan is the acquisition of a single interferogram when the mobile mirror of the Michelson interferometer begins data collection at the Zero Path Difference (ZPD) and finishes at the maximum length, therefore achieving the highest resolution required. In Fig.~~??~~2, the spectrum with 10 scans has a higher amplitude than that of 50 and 100 scans. On the other hand, ~~if we look closely,~~ the spectra of 50 and 100 scans are clearly less noisy than that of the 10 scans. This is due to the fact that the increase in the number of scans causes an increase in the SNR which leads to the decrease of the noise. However, there is a limit to the number of scans beyond which no improvement of the SNR is obtained. The SNR is proportional to the square root of the acquisition time (number of scans), also known as the Fellgett's advantage and since the detector is shot noise dominated, the improvement of the SNR with the number of scans is blocked at a certain value, and this is why the spectra of ~~50 and~~ 100 and 200 scans do not ~~have a big difference.~~ show a significant difference. The SNR is an estimation of the root mean squared noise of the covered spectral domain and can be calculated in OPUS (the running program for CHRIS) using the function SNR with option fit parabola; it is estimated to be approximately 780. An optimized criteria is chosen to select the appropriate number of scans: when the wanted species has a fast changing concentration, such as volcanic plumes, a relatively small number of scans is needed to be able to follow temporally the change in the atmospheric composition; while in contrast, when measurements of relatively stable atmospheric composition are made, for example GHG (CO_2 and CH_4), the number of scans can be increased to 100. For instance, the time needed for 1 scan with a scanning velocity of 120 KHz is 0.83s, so 100 scans take approximately 83s which is low in comparison with the variability of CO_2 and CH_4 in the atmosphere.

Another important feature is the effect of the gain amplitude (and pre-amplifiers) on the spectra, which plays the role of

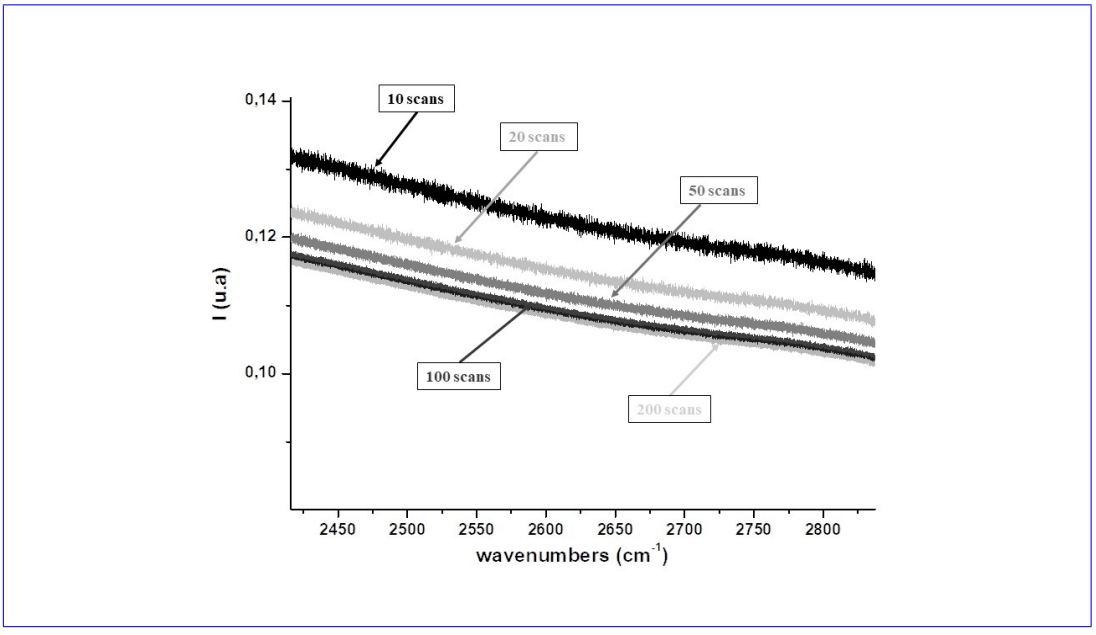

Fig. 2: Improvement of the SNR with different scan numbers and a fixed scan speed of 120 KHz.

amplifying the signal before digitization. Those parameters should be chosen in a way that the numeric count, falls in a region where no detector saturation occurs. If the gain is increased of a certain amount, the background noise is increased by the same amount. The use of such an option in the measurement procedure might be considered in cases where the signal is very weak, like the lunar measurements. Note that there are other ways to increase the intensity of the signal like using signal amplifying filters (see Section 2.1), or increasing the aperture stop diameter.

2.3.1 ~~Measurement~~

~~CHRIS's method of data acquisition is explained as follows: the interferograms are sampled and digitized by an Analogue-to-Digital Converter (ADC), and then numerically resampled at constant intervals of OPD by a He-Ne reference laser signal controlled by the aperture stop diameter. In order to determine a suitable compromise between the latter and to avoid the saturation of the signal, measurements must be done in a clear (no clouds or aerosols) and non-polluted (no gases with high chemical reaction) atmosphere. For this purpose, a field campaign was carried out at the "El Observatorio Atmosférico de Izaña" (28.30°N, 16.48°W) in the Tenerife island. This particular observatory site is high in altitude (2374 m), away from pollution sites and has an IFS125HR listed in both the NDACC and TCCON networks. Saturation of the CHRIS's detector is reached at a value of 32000 ADC. The MCT detector is known for its high photometric accuracy but it also exhibits a non-linear response with regard to the energy flux in cases of high incident energy. This led us to choose an aperture stop of 5 mm, which is the best compromise between saturation and incoming energy flux. In the~~

2.4 Radiometric and spectral calibration

In the following section, the spectral and radiometric calibrations are discussed in order to convert spectra from numeric counts expressed in arbitrary units to radiance expressed in $W.m^{-2}.sr^{-1}.cm$. ~~An example of the spectra recorded by CHRIS is shown in Fig. 3 where the spectral range spans the region from 680 to 5200 cm^{-1}. The water vapor causes the saturation we see between the bands, thus the 0 signal. Therefore, we divided the spectrum into 4 distinctive spectral bands presented in Table 3: BT (thermal band: 680-1250 cm^{-1}), B1 (1800-2300 cm^{-1}), B2 (2400-3600 cm^{-1}) and B3 (3900-5200 cm^{-1}) and this annotation is used for the rest of the paper.~~

2.4.1 ~~Spectral and radiometric~~ Radiometric calibration

~~The sampling of the interferogram is controlled by a standard, not frequency-stabilized He-Ne laser with a wavelength of 632.8 nm which serves as a reference while converting from the distance scale to the wavenumber scale. This reference wavelength~~

changes in function of the pressure and temperature conditions in which the instrument is placed in, thus the refractive index will change which will lead to an instability in the conversion process and therefore the need for a spectral calibration to reduce this error. To do so, we choose isolated lines in the spectra and apply Eq.4 which is limited by a 0.038 cm^{-1} maximum precision. A Sinc wavefunction is used to re-simulate these absorption lines from the Hitran (Gordon et al. (2017)) database considering non-apodized spectra which allows the exploitation of the full spectral resolution. In short, we choose an intense, non-saturated and always present in the spectra absorption line of H_2O with wavenumber ν, then we compare it with the simulation and calculate its new wavenumber ν^*:

$$\nu^* = \nu(1+\alpha)$$

where α is the calibration factor.Despite the fact that CHRIS has an internal blackbody, radiometric calibration cannot be overlooked because of its narrow spectral coverage (only the TIR region), and since the radiometric noise, time dependent and wavelength dependent calibration errors are magnified in the inversion process, high radiometric precision is required to derive atmospheric parameters from a spectrum. We calibrate our spectra using the two points calibration method explained in Revercomb et al. (1988). This method consists of using the observations of hot and cold blackbody reference sources which will be used as the basis for the two points calibration at each wavenumber. A cavity blackbody (SR-2 from CI systems) that can be heated up to 1473 K, is used was acquired by the LOA to perform regular radiometric calibrations. The latter is an HGH/RCN1250N2 certified by the LNE (Laboratoire National de métrologie et d'Essais) as having an emissivity greater than 0.99 in the spectral domain spanned by CHRIS, a stability of 0.1 K at 1173 K, an opening diameter up to 50 mm (corresponding to that of CHRIS), and covering temperatures from 323 to perform this experiment. These 2 1523 K. This cavity blackbody is mounted on an optical bench and used before and after each campaign to perform absolute radiometric calibrations through open path measurements and make sure that this calibration is stable across the whole spectral range. These two blackbody temperatures are viewed to determine the slope m and offset b (Eq. 1 & 2) which defines the linear instrument response at each wavenumber. The slope and the offset can be written asfollowing Revercomb et al. (1988):

$$m = \frac{S_c - S_h}{B_\nu(T_c) - B_\nu(T_h)} \tag{1}$$

$$b = \frac{S_c * B_\nu(T_h) - S_h * B_\nu(T_c)}{B_\nu(T_h) - B_\nu(T_c)} \tag{2}$$

where S is the blackbody spectrum recorded and B_ν corresponds to the calculated Planck blackbody radiance; the subscripts h and c corresponds respectively to the hot and cold (1473 K) and cold (1273 K) blackbody temperatures. Finally, the calibrated spectrum expressed in radiance $W.m^{-2}.sr^{-1}.cm$ is obtained by applying the following formula:

$$L = \frac{S - b}{m} \tag{3}$$

where S is the spectrum recorded by CHRIS. In the retrieval of gases, the spectrometer's line-of-sight (LOS) has to be known for calculating the spectral absorption of the solar radiation while passing through the atmosphere. For this, the time and the duration of each measurement is saved, from which the required effective solar elevation (respectively the Solar Zenith Angle (SZA)) is calculated based on the routine explained in Michalsky (1988).

2.4.2 Instrumental Line Shape (ILS) and spectral calibration

One open path measurement using the calibrated HGH blackbody as source was performed, similar to the one previously described in Wiacek et al. (2007), to record a spectrum without applying any apodization. Our colleagues in the PC2A laboratory provided us with a 10-centimeter-long cell, with a free diameter of 5 cm where the pressure inside is monitored by a capacitive gauge. With the help of the line-by-line radiative transfer algorithm, ARAHMIS (Atmospheric Radiation Algorithm for High-spectral Measurements from Infrared Spectrometer), developed at the LOA laboratory an MOPD of 4.42 cm was determined corresponding to a spectral resolution of 0.135 cm^{-1} using a sinc function with a spectral sampling every 0.06025 cm^{-1} to satisfy the Nyquist criterion. In FTIR spectroscopy, a poor ILS determination generates a significant error in the retrieval process, so we are currently modifying the optical bench in order to perform an ILS determination at the same time as the radiometric and spectral calibrations before each field campaign.

Moreover, accurate knowledge of the solar radiance in the IR region is required to validate our results since the sun is the initial source of CHRIS. Trishchenko (2006) offered a detailed and extensive study on the matter, and combined the work of

four recent solar reference spectra . In our work, two of these reference spectra with 0.1% relative difference are taken into consideration: Kurucz and the American Society of Testing and Materials (ATSM). These solar references agree on one point: The sampling of the interferogram is controlled by a standard, not frequency-stabilized He-Ne laser with a wavelength of 632.8 nm which serves as a reference while converting from the distance scale to the wavenumber scale. The instrument is subjected to changes in pressure and temperature since it operates in different locations, therefore in different meteorological conditions. This will cause a change in the refractive index and as a consequence a change in the reference wavelength of the laser which will lead to an instability in the conversion process and therefore the need for a spectral calibration to reduce this error. The ILS line defined above is used to re-simulate isolated absorption lines from the HITRAN database (Gordon et al. (2017)) considering non-apodized spectra which allows the exploitation of the effective brightness temperature depends strongly on the wavenumber. Based on these findings, the Planck function is calculated in each spectral domain of CHRIS, and then adjusted by a polynomial fit. The final calibrated spectrum is shown in Fig. 3. full spectral resolution. In short, we choose an intense, non-saturated and always present in the spectra absorption lines of H_2O with wavenumber ν, then we compare it with the simulation and calculate its new wavenumber ν^*:

$$\nu^* = \nu(1+\alpha) \tag{4}$$

where α is the calibration factor. Eq.4 is limited by a 0.038 cm^{-1} precision, corresponding to roughly half of the spectral sampling, estimated from the standard deviation between the theoretical HITRAN spectroscopic lines and the measured ones by CHRIS. Fig. 3 shows the comparison between a calibrated and a non-calibrated spectrum along with the solar Planck function explained in Section 3.1. Spectral and radiometric calibrations procedure is automated using a Matlab code to convert the spectra instantly from numeric counts to absolute radiance.

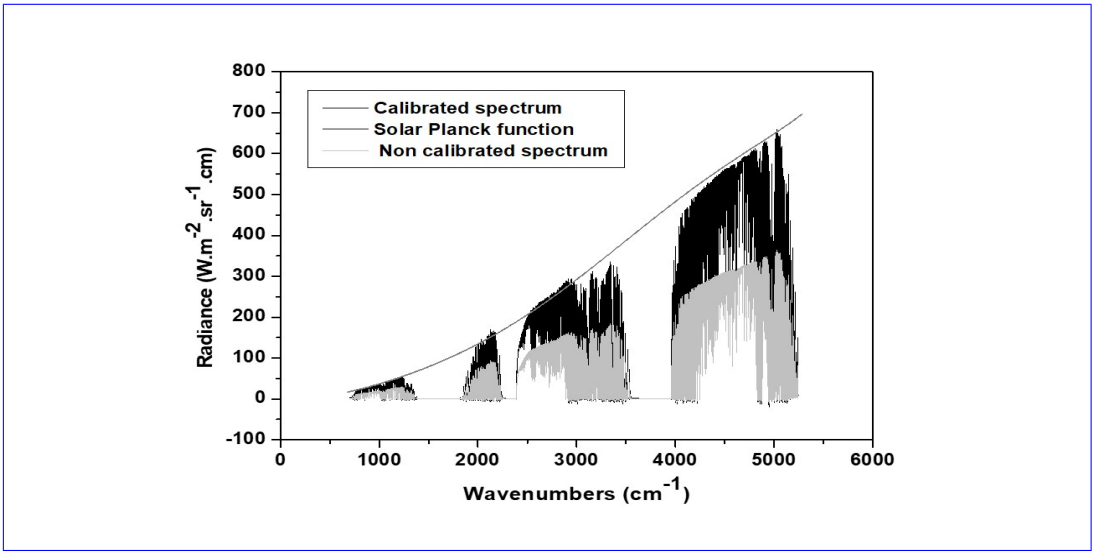

Fig. 3: CHRIS spectrum after calibration. The simulation with ARAHMIS calibration process transforms the non-calibrated spectrum (blacklight gray) reproduce the into a calibrated spectrum one (greenblack) and that fits with the solar Planck function (solid blue gray line).

2.5 Radiometric stability

During campaigns and after long transportations, constant measurements of the internal blackbody, which can be heated up to 353 K, is carried out in the thermal infrared region (most affected by drifts). Figure 4 shows the variations of the internal blackbody during multiple field campaigns: a little fluctuation in function of the measurement conditions can be seen, but depending on the locations and even years, no systematic drift can be detected, so we can safely say that the instrument is quite stable between each laboratory calibration.

2.6 Spectral artifacts

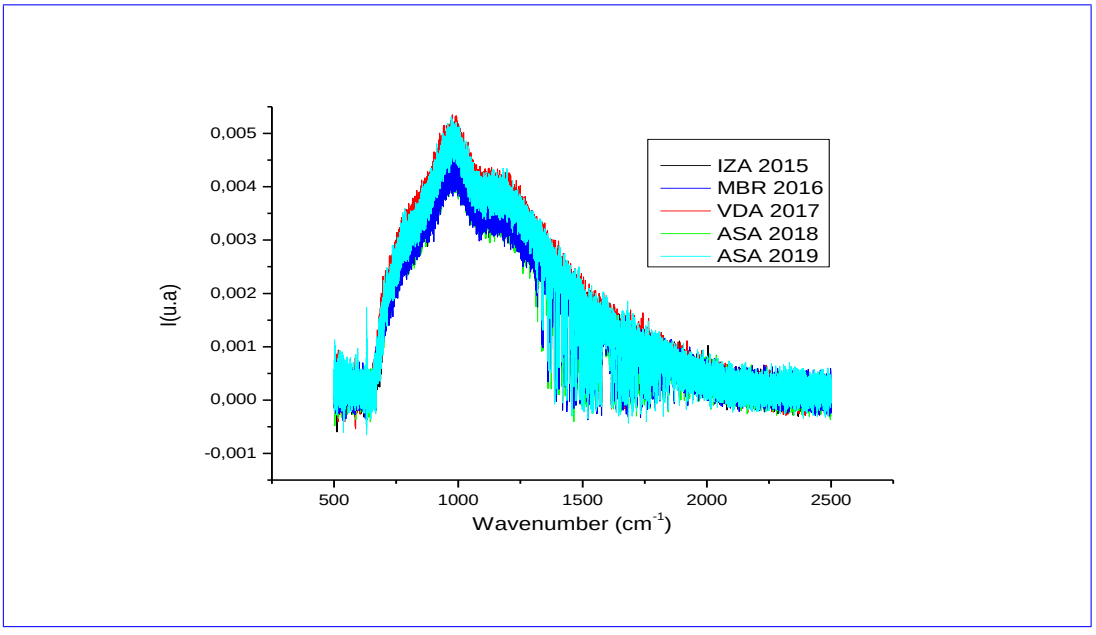

Fig. 4: ~~Measured and simulated CHRIS spectrum in transmittance for clear sky conditions at Izaña observatory. Each band~~ The radiometric stability of the instrument is ~~calculated from~~ achieved by following the ~~line-by-line forward model ARAHMIS~~variations of the internal blackbody during multiple field campaigns. IZA : Izana, MBR : M'Bour, VDA : Villeneuve d'Ascq, ASA : Aire-sur-l'Adour.

There are commonly several well-known spectral artifacts: the aliasing, the picket-fence effect also known as the resolution bias error, and the phase correction, which are well controlled in CHRIS.

An aliasing is the result of the missampling of the interferogram in the x-axis locations, which leads to errors in the retrieved column abundances due to its overlap with the original spectrum. The He-Ne laser, having a wavelength λ of 632.8 nm, generates the sampling positions of the interferogram at each zero crossing. No overlap will occur if the signal of the spectrum is 0 above a maximum wavenumber ν_{max} and if ν_{max} is smaller than the folding wavenumber $\nu_f = 1/(2.\Delta x)$. Since $\Delta\nu$ is related to the sample spacing Δx, the minimum possible Δx is 1/31600 cm, since each zero crossing occurs every $\lambda/2$. This corresponds to a folding wavenumber of 15800 cm^{-1}, i.e. the maximum bandwidth that can be measured without overlap has a width of 15800 cm^{-1}. This source error is of special relevance to the spectra acquired in the Near Infrared region. However, for the MIR, the investigated bandwidth is much smaller than 15800 cm^{-1}, where ν_{max} is less than 5200 cm^{-1} so CHRIS's spectra are not affected by this problem (Dohe et al. (2013)).

The picket-fence effect, or the resolution bias error, becomes evident when the interferogram contains frequencies, which do not coincide with the frequency sample points, but this is overcome in our spectra by the classical method of the Zero Filling Factor (ZFF) where zeros are added to the end of the interferogram before Fourier Tranform is performed, thereby doubling the size of the original interferogram.

The phase correction is necessary while converting the interferogram into a spectrum, which is relevant to single-sided measurements, similar to those acquired by CHRIS. Mertz phase correction is the method used for CHRIS to overcome this problem, which relies on extracting the real part of the spectrum from the complex output by multiplication of the latter by the inverse of the phase exponential, therefore eliminating the complex part of the spectrum generated.

Besides these classical FTIR artefacts, we noticed during our tests that when using a scan speed of 160 KHz, we drastically increase the non-linearity effect of the detector (see Fig. 5). However, we identified a ghost signal for low scanning velocities (for example 40 KHz shown in Fig. 6). This ghost is specific to CHRIS because it is caused by the noise introduced from the vibrations of the compressor used in the closed-cycle Stirling cooler as mentioned in Sect. 2.1. The choice of a scanning velocity of 120 KHz is a compromise between two important features: the elimination of the ghost signal, which appears at scanner velocities below 80 KHz, and the increase of the detector non-linearity at a velocity of 160 KHz.

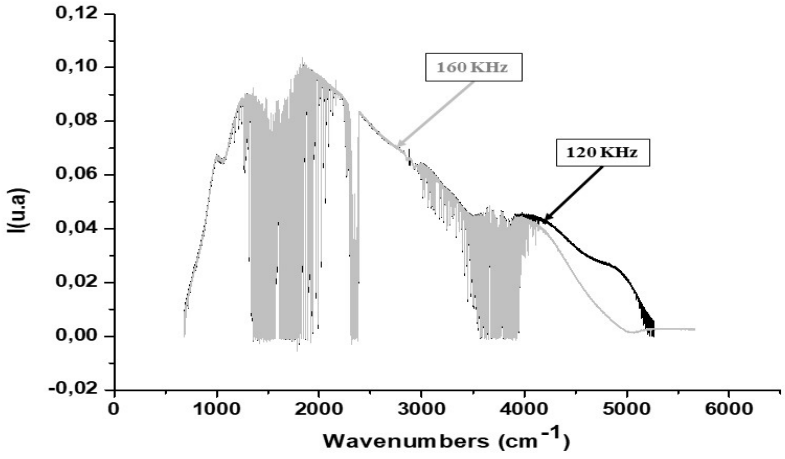

Fig. 5: Spectra of the external blackbody with two different scanning velocities: 120 KHz (black) and 160 KHz (light gray).

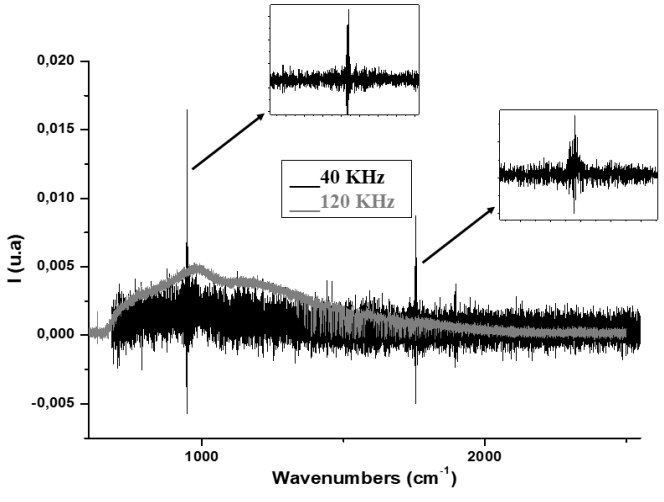

Fig. 6: Spectra of the internal blackbody of CHRIS with scanner velocities of 40 KHz (black) and 120 KHz (light gray).

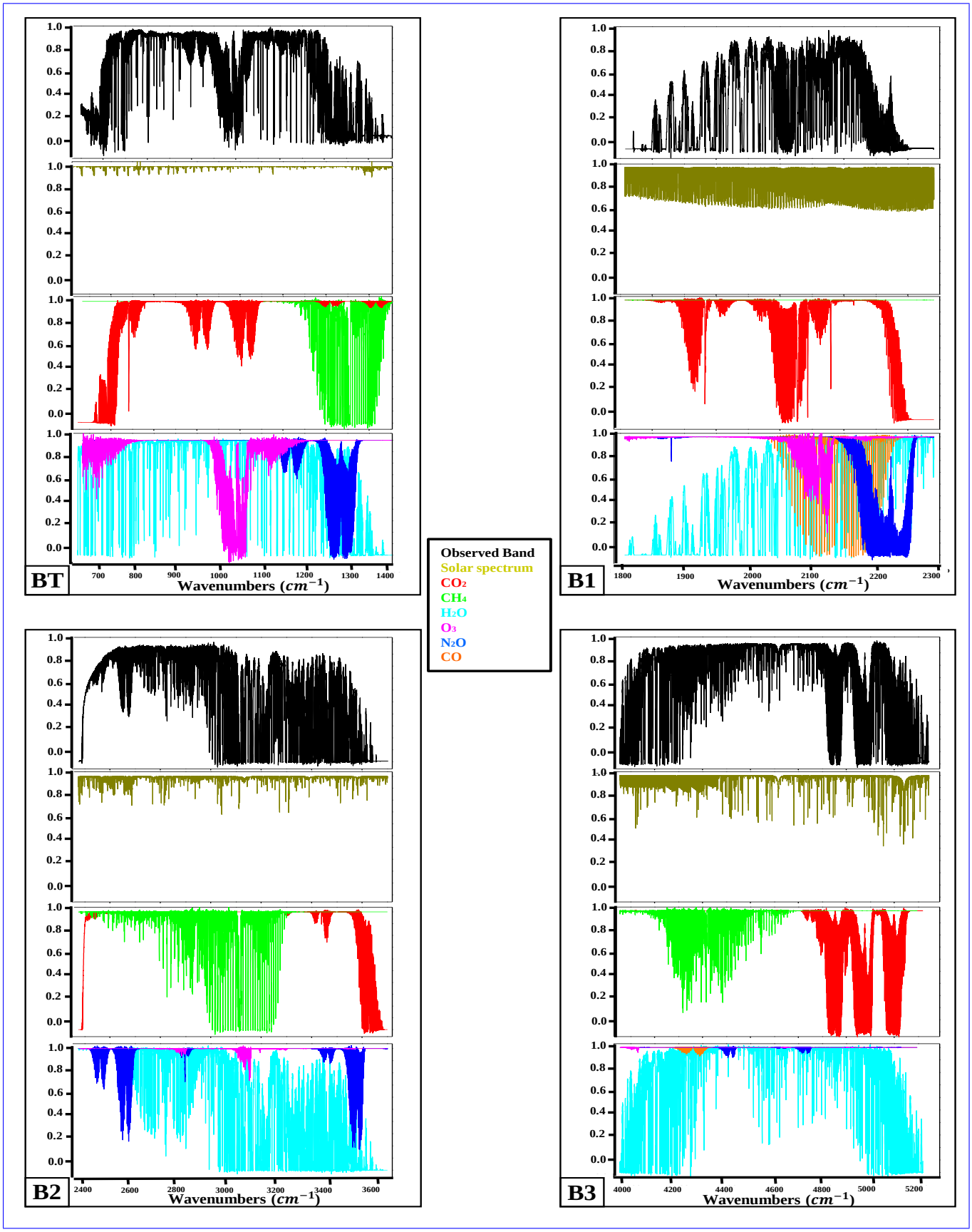

Fig. 7: Measured and simulated CHRIS spectrum in transmittance for clear sky conditions at Izaña observatory. Each band is calculated from the line-by-line forward model ARAHMIS and the solar pseudo-transmittance spectra reported by Toon (2015)

3 Information content analysis

~~The MAGIC campaigns are a french initiative supported by the CNES, that serve as a way of understanding the vertical exchange of the GHG (CO_2 and CH_4) along the atmospheric column through multi-instruments such as satellites, lidar, balloons and ground-based measurements. In this context, CHRIS is one of the instruments used in these campaigns and since it's a~~ Since CHRIS is an instrumental prototype, its ability to retrieve ~~these~~ GHG is unknown; ~~hence~~ therefore it is important to perform an information content ~~analysis to quantifythe quality of retrieval of these gases~~study to quantify, in a first attempt, its potential capability to retrieve GHG. In this context, CHRIS is one of the instruments deployed in the MAGIC project alongside satellites, lidar, balloons and ground-based measurements. The latter is a French initiative supported by the CNES (Centre National d'Etudes Spatiales), which aims to implement and organize regular annual campaigns in order to better understand the vertical exchange of the GHG (CO_2 and CH_4) along the atmospheric column and establish a long-term validation plan for the satellite level 2 products.

3.1 The forward model

Accurate calculations of the ~~radiance~~ radiances observed by CHRIS ~~(then divided by the Planck function to obtain the transmittance)~~ are achieved with ~~a~~ the line-by-line radiative transfer algorithm ARAHMIS ~~, developed at the Laboratoire d'Optique Atmosphérique (LOA),~~ over the thermal and ~~solar infrared spectral regions~~ shortwave infrared spectral range (1.9-14.7 µm). Gaseous absorption is calculated ~~with ARAHMIS~~ based on the updated HITRAN 2016 database (Gordon et al. (2017)). The absorption lines are computed assuming a Sinc line shape and no-apodization is applied which allows the exploitation of the full spectral resolution. In this study, the term "all bands" refers to the use of the bands BT, B1, B2 and B3 simultaneously of CHRIS (see Section ~~??~~2.2). Absorption continua ~~(~~for H_2O and CO_2 ~~)~~ are also included ~~. The solar~~ from the MT-CKD model (Clough et al. (2005)). The pseudo-transmittance spectra corresponding to direct sunlight from the center of the solar disk reported by Toon (2015) is used as the incident solar spectrum ~~.~~ interpolated on the spectral grid of CHRIS. The effective brightness temperature depends strongly on the wavenumber, thus the Planck function is calculated in each spectral domain of CHRIS determined from Trishchenko (2006) who combined the work of four recent solar reference spectra. Two of these reference spectra with 0.1% relative difference are taken into consideration, and then adjusted by a polynomial fit (solid line in Fig. 3). In the gaseous retrieval process, the spectrometer's line-of-sight (LOS) has to be known for calculating the spectral absorption of the solar radiation while passing through the atmosphere. For this, the time and the duration of each measurement is saved, from which the required effective solar elevation (respectively the Solar Zenith Angle (SZA)) is calculated based on the routine explained in Michalsky (1988).

As mentioned in Section 3.3.2, $Izaña$ offers clear non-polluted measurements since it is high in altitude and away from major pollution sites, so calculations are performed based on the concentration of the desired atmospheric profile with the corresponding profile information~~including the temperature~~: the temperature, pressure and relative humidity are derived from the radiosondes (http://weather.uwyo.edu/upperair/sounding.html); CO_2 and ~~humidity.~~CH_4 profiles are derived from the TCCON database, whereas O_3, N_2O and CO concentrations are calculated from a typical mid-latitude summer profile. Figure 7 shows the results of the forward model simulation superimposed with the four infrared bands measured by CHRIS. For each band, we present the influence of the solar spectrum, the GHG ~~in question~~ (CO_2 and CH_4) and the major ~~molecular absorbers in the atmosphere that are not included in our potential inversion process~~interfering molecular absorbers. We can ~~clearly see that with the help of ARAHMIS, CHRIS's signal is very well re-simulated~~ see the good agreement between ARAHMIS's simulations and the CHRIS measurements in clear sky conditions.

3.2 Information ~~content~~ Content (IC) theoretical basis

Once the forward model is calculated, we ~~will~~ rely on the formalism of Rodgers (2000) that introduces the optimal estimation theory used for the retrieval, which is widely ~~known elsewhere and summarized here~~described elsewhere (e.g. Herbin et al. (2013a)) and summarized hereafter.

In the case of an atmosphere divided in discrete layers, the forward radiative transfer equation gives an analytical relationship between the set of observations y (in this case, the radiance) and the vector of true atmospheric parameters x (i.e. the variables to be retrieved: vertical concentration ~~profile~~ profiles of CO_2 and/or CH_4):

$$y = F(x; b) + \varepsilon, \tag{5}$$

where F is the forward radiative transfer function (here the ARAHMIS code), b represents the fixed parameters affecting the measurement (e.g. atmospheric temperature, ~~surface emissivity~~interfering species, viewing angle, etc.) and ε is the measurement

~~errors~~ error vector.
In the following information content study, two matrices fully characterize the information provided by CHRIS: the averaging kernel A and the total error covariance S_x~~, fully characterize the information provided by CHRIS~~.
The averaging kernel matrix A, gives a measure of the sensitivity of the retrieved state to the true state, and is defined by:

$$A = \partial\hat{x}/\partial x = GK, \tag{6}$$

where K is the Jacobian matrix (also known as the weighting function), where the ith row is the partial derivatives of the ith measurement with respect to each (j) element of the state vector: $K_{ij} = (\partial F_i/\partial x_j)$, and K^T is its transpose.
The gain matrix G , whose rows are the derivatives of the retrieved state with respect to the spectral points, is defined by:

$$G = \partial\hat{x}/\partial y = (K^T S_\varepsilon{}^{-1} K + S_a^{-1})^{-1} K^T S_\varepsilon^{-1}, \tag{7}$$

where S_a is the a priori covariance matrix describing our knowledge of the state space prior to the measurement and S_ϵ represents the forward model and the measured signal error covariance matrix.
At a given level, the peak of the averaging kernel row gives the altitude of maximum sensitivity, whereas its full width at half maximum (FWHM) is an estimate of the vertical resolution. The total Degrees Of Freedom for Signal (DOFS) is the trace of A, which indicates the amount of independent pieces of information that one can extract from the observations with respect to the state vector. A perfect retrieval resulting from an ideal inverse method would lead to an averaging kernel matrix A equal to the identity matrix with a DOFS equal to the size of the state vector. Therefore, each parameter we want to retrieve is attached to the partial degree of freedom represented by each diagonal element of A.
The second important matrix in the IC study is the error covariance matrix S_x, which describes our knowledge of the state space posterior to the measurement. Rodgers (2000) demonstrated that this matrix can be written as:

$$S_x = S_{smoothing} + S_{meas\,meas.} + S_{fwd.mod\,fwd.mod.} \tag{8}$$

From Eq.8, the smoothing error covariance matrix $S_{smoothing}$ represents the vertical sensitivity of the measurements to the retrieved profile:

$$S_{smoothing} = (A - I)S_a(A - I)^T \tag{9}$$

$S_{meas.}$ gives the contribution of the measurement error covariance matrix through S_m which illustrates the measured signal error covariance matrix, to the posterior error covariance matrix S_x. S_m is computed from the spectral noise:

$$S_{meas.} = GS_mG^T \tag{10}$$

At last, $S_{fwd.mod.}$ and gives the contribution of the posterior error covariance matrix through S_f the forward model error covariance matrix, which illustrates the imperfect knowledge of the non-retrieved model parameters:

$$S_{fwd.mod.} = GK_bS_b(GK_b)^T = GS_fG^T \tag{11}$$

with S_b representing the error covariance matrix of the non-retrieved parameters.

3.3 A priori information

The IC analysis uses simulated radiance spectra of CHRIS in the bands: BT, B1, B2 and B3. The CO_2 and CH_4 vertical concentrations of the a priori state vector x_a are based on a profile that follows the criteria described in Section 3.1 ~~divided by 20 vertical levels~~discretized by 40 vertical layers, extending from the ground to ~~20~~ 40 km height with 1 km step. In addition, the water vapor vertical profile~~and the temperature~~ , the temperature and the SZA are included in the non-retrieved parameters and ~~will be~~ are discussed in Section 3.3.3. The a priori values and their variabilities are summarized in Table 1 and ~~will be~~ are described in the following ~~section~~sections.

3.3.1 A priori error covariance matrix

In situ data or climatology can give us an evaluation of the a priori error covariance matrix S_a. ~~Nevertheless, the correlation of the vertical layers is more expressed by the off-diagonal matrix elements.Since~~ Since the use of diagonal a priori covariance matrices is common for the retrievals from space measurements (e.g. De Wachter et al. (2017)), and since this study is dedicated

to information coming from the measurement rather than climatology's or in situ observations, we ~~will always assume~~ assume firstly that S_a ~~as~~ is a diagonal matrix with the ith diagonal element ($S_{a,ii}$) defined as:

$$S_{a,ii} = \sigma_{a,i}^2 \quad \text{with} \quad \sigma_{a,i} = x_{a,i}.\frac{p_{error}}{100} \tag{12}$$

where $\sigma_{a,i}$ stands for the standard deviation in the Gaussian statistics formalism. The subscript i represents the ith parameter of the state vector. The CO_2 profile a priori error is estimated from Schmidt and Khedim (1991). The CH_4 a priori error is fixed to p_{error}=5% similar to the one used in Razavi et al. (2009) for the ~~inversion of the data~~ retrieval of the methane obtained from IASI ~~.~~ and also to be consistent with the previous study concerning the TANSO-FTS instrument (Herbin et al. (2013a)). Nevertheless, the correlation of the vertical layers is more expressed by the off-diagonal matrix elements. This is the reason we also use an a priori covariance matrix similar to the one used in Eguchi et al. (2010), where the climatology derived from TCCON is used to construct this matrix. The study with these two covariance matrices is presented for CHRIS in the following sections.

State vector elements	T	H_2O	SZA	CO_2	CH_4
a priori values ~~x_a~~	Radiosondes	~~US standard~~ Radiosondes	10°/80°	TCCON database	TCCON database
A priori uncertainty (P_{error})	1 K/layer	10%	0.35°	1.3-8%	5%

Table 1: State vector parameters.

3.3.2 Measurement error covariance matrix

The measurement error covariance matrix is computed knowing the instrument performance and accuracy. The latter is related to the radiometric noise expressed by the SNR already discussed in Section ~~??~~2.3. This error covariance matrix is assumed to be diagonal, and the ith diagonal element can be computed as follows:

$$S_{m,ii} = \sigma_{m,i}^2 \quad \text{with} \quad \sigma_{m,i} = \frac{y_i}{SNR}, \tag{13}$$

where $\sigma_{m,i}$ is the standard deviation of the ith measurement (y_i) of the measurement vector y, representing the noise equivalent spectral radiance. The SNR for CHRIS is ~~found~~ estimated to be 780 and it is reported with other instrumental characteristics in Table 3.

3.3.3 Non-retrieved parameter characterization and accuracy

The effects of non-retrieved parameters is a complicated part of an error description model. In our case these uncertainties are limited to the interfering water vapor molecules due to its important existence in the spectra and the effect of the temperature, where a vertically uniform uncertainty is assumed in both cases. It is important to note that in this study the water vapor is considered as a non-retrieved parameter, for the sake of comparison with Herbin et al. (2013a), but it will be part of the retrieved state vector in the inversion process which will be the subject of a future study.
On one hand, we assumed a partial column with an uncertainty (p_{Cmol}) of 10% instead of a profile error for H_2O. On the other hand, we assumed a realistic uncertainty of $\delta T = 1K$, compatible with the typical values used for the ECMWF assimilation, on each layer of the temperature profile. Moreover, we assumed a realistic uncertainty of 0.35° on the SZA, corresponding to the difference in the solar angle during the acquisition of a measurement corresponding to 100 scans. All these variabilities are reported in Table 1.
The total forward model error covariance matrix (S_f), assumed diagonal in the present study, is given by summing the contributions of each diagonal element, and the ith diagonal element ($S_{f,ii}$) is given by:

$$S_{f,ii} = \sum_{j=1}^{nlevel} \sigma_{f,T_j,i}^2 + \sigma_{f,H_2O,i}{}^2 + \sigma_{f,SZA,i}^2 \tag{14}$$

Here, the spectroscopic effects such as the line parameter, the line mixing and the continua errors are not considered but they are discussed with the X_G column estimation in Section 3.4.2.

3.4 Information content analysis applied to greenhouse gases profiles

An information content analysis is performed on the whole spectrum for CO_2 and CH_4 separately to quantify the benefit of the multispectral synergy. Separately means that the state vector is constituted of only one of the above gas concentrations at each level between 0 and ~~20 km~~ 40 km to match the altitudes reached by TCCON and the MAGIC instruments (balloons and planes reaching altitudes of more than 25 km). This corresponds to the case where we estimated each gas profile alone when all other atmospheric parameters and all other gas profiles are known from ancillary data with a specific variability or uncertainty. Two different SZA (10° and 80°) are chosen to demonstrate the effect of the solar optical path on the study since the sensitivity is correlated to the viewing geometry. Furthermore two different a priori covariance matrices are used to show the effect of using climatological data describing the variability of GHG profiles. In the following subsections, we explain in details the averaging kernel, error budget and total column estimations.
~~Figure 8 and 9 show~~

3.4.1 Averaging kernel and error budget estimation

Figure 8 shows the averaging kernel A and total posterior error S_x for CO_2 ~~and CH_4 respectively~~ for an angle of 10°. The ~~same is done for~~ figures of the second SZA (80°~~and is used only to compare with the results of the 10° angle~~) are not shown since the vertical distribution of the kernels and errors is quite similar and exhibits only slight differences in the amplitude with respect to the other angle. However, the results are different, this is why they are discussed in order to quantify the information variability with the viewing geometry. A is obtained for ~~each greenhouse gas~~ CO_2 independently using the variability introduced in Section 3.3.1, and considering an observing system composed of the band BT, B1, B2 or B3 separately and all the bands together to quantify the contribution of each of the spectral bands and show the benefits of the TIR/SWIR spectral synergy. Each colored line represents the row of A at each vertical grid layer. Each peak of A represents the partial degree of freedom of the gas at each level that indicates the proportion of the information provided by the measurement. In fact, if the value is close to unity, it means that the information comes predominantly from the measurement, but a value close to zero means that the information comes mainly from our prior knowledge of the ~~system (~~a priori state~~). For CO_2, for an angle of~~ . We can clearly see that at lower altitudes and up to 10 ~~°, the total DOFS are 2.56, 2.42, 3.12 and 3.52 for the bands BT, B1, B3 and all bands respectively and for an angle of 80° the DOFS are 2.6, 2.74, 3.46 and 3.79 for the same bands . This parameter show that one might be able to retrieve between 3 and 4 partial tropospheric columns for CO_2, and as expected the DOFS is slightly higher at 80° since the optical path of the sun in every layer is longer. Fig.8 shows that the~~ km, the kernels are close to unity suggesting that the measurement improved our knowledge, while at higher altitudes (beyond 10 km) the kernels are close to 0. It is important to also note that when using all the bands simultaneously, the information distribution of the kernels is improved and is more homogeneous along the vertical profile.
The measurement may provide information about CO_2 ~~arises~~ from the ground ~~to 12~~ up to 20 km high in the atmosphere (all bands), while at much higher altitudes the information comes mainly from the a priori, due to a smaller sensitivity ~~to CO_2~~ of these gases in the upper troposphere. This is ~~also shown~~ clearly represented in the error budget study: ~~in the lower part of the atmosphere (between 0 and 12 km), the~~ the a posteriori total error (solid black line) is significantly smaller than the a priori error (red line) in the lower part of the atmosphere (between 0 and 20 km), which means that the measurement improved our knowledge of the CO_2 profile; while beyond ~~12~~ 20 km, the total a posteriori error is equal to the a priori error suggesting a very poor sensitivity at high altitudes. ~~Also, the vertical information distribution is improved when all the bands are used simultaneously.~~ Furthermore, one can notice that the measurement error stays very weak regardless of the band used which proves that ~~our SNR is largely sufficient and does not limit the inversion process~~the error related to the SNR is negligible. Also, the forward model error depending on the non-retrieved parameters remains quite modest. However, the smoothing error predominates the other errors and becomes preponderant beyond ~~12~~ 20 km, which means that the information is strongly constrained by the a priori profile at high altitudes, and little information is introduced from the measurement. ~~The same reasoning is presented for CH_4: for an angle of~~ To overcome this problem, another similar study was conducted but with a non-diagonal a priori covariance matrix (Eguchi et al. (2010)). The vertical distribution is more homogeneous through all the layers. The shape of the error budget is very similar to that of the variance; however, the a priori and a posteriori errors are significantly reduced. The measurement and forward model errors remain weak, but it is important to note that despite the fact that the smoothing error is smaller, the constraint is stronger. This has the effect of decreasing the uncertainty, but increasing the propagation of the smoothing error along the vertical layers, which explains the smaller values of the DOFS.
Finally, the total DOFS for CO_2 are shown in Table 4 for angles of 10°~~, the total DOFS, for bands BT, 2, 3 and all bands respectively are: 3.16, 3.55, 2.82 °~~ and ~~3.86; and for an angle of~~ 80°~~the DOFS for the same bands are: 3.28, 3.95, 3.53 and 4.27. These slightly better values show that retrieving tropospheric columns~~ . It shows that, for a diagonal a priori covariance matrix, one might be able to retrieve between two and three partial troposheric columns for CO_2, and as expected the DOFS is slightly

higher at 80° since the optical path of the sun in every layer is longer. However, when using a non-diagonal a priori covariance matrix, one less partial tropospheric column is retrieved but with significant improvement in the error budget estimation.
The same reasoning is followed for CH_4 ~~from such measurements is as efficient as CO_2~~: A is obtained for CH_4 independently using the variability introduced in Section 3.3.1, and considering an observing system composed of the band BT, B1, B2 or B3 separately and all the bands together. Fig.9 shows that the vertical distribution of CH_4 is more homogeneous than that of CO_2 and we can see that the A's are broader than those of CO_2, suggesting a very important correlation between layers. The use of all the bands simultaneously, just like CO_2, improves the information distribution along the vertical profile. The forward model error is ~~systematically weaker than the measurement error , unlike~~ larger than that of CO_2 since the methane is more affected by the interfering species. The smoothing error is significantly larger than CO_2, ~~due to the fact that the methane bands are less impacted by the interfering molecules, especially H_2O (see Fig. 7)~~since it is constrained by a much higher a priori, which suggests a more direct effect on the retrieval of CH_4. Similarly to CO_2, when using a non-diagonal a priori covariance matrix, the vertical distribution is very analogous to that of the variance only. However, the a priori and a posteriori errors are significantly reduced. The total DOFS for CH_4 are shown in Table 5 for both SZA. This parameter shows that, for a diagonal a priori covariance matrix, three partial tropospheric columns can be retrieved, and one additional partial column for a SZA of 80°. Finally, while using a non-diagonal a priori covariance matrix the DOFS shows that one less partial column is retrieved.
As a general result, the simultaneous use of all the bands instead of using each one separately increases the total DOFS and reduces systematically the total errors of the two species. Moreover, using a climatological a priori covariance matrix shows the importance of reducing the error of the retrieved partial columns. Finally, the total profile error is derived from the relative values of the diagonal matrix of S_x ~~. The~~ (see Tables 4 and 5), which are discussed in details in the following section.

3.4.2 Total column estimation and uncertainty

Ground-based instruments like the one used in the TCCON network and the EM27/SUN operate in the NIR, where the column-averaged dry-air mole fractions (denoted X_G for gas G) is calculated by monitoring the observed O_2 columns. X_G is calculated by rationing the gas retrieved slant column to the O_2 retrieved slant column for the same spectrum. Another method is used, especially among the NDACC community, to calculate X_G without using the oxygen reference. Based on the formula given in Wunch et al. (2011) and used in Zhou et al. (2019), we can calculate X_G for CO_2 ~~total profile error for CHRIS is estimated to be 2.62%, whereas the CH_4 total profile error is 4.22% . Clearly,~~ and CH_4:

$$X_G = \frac{column_G}{column\,dry\,air} \tag{15}$$

$$column\,dry\,air = \frac{P_s}{g_{air} m_{air}^{dry}} - column_{H_2O} \frac{m_{H_2O}}{m_{air}^{dry}}$$

Where m_{H_2O} and m_{air}^{dry} are the mean molecular masses of water and dry air, respectively, P_s the surface pressure and g_{air} the column-averaged gravitational acceleration. Therefore, the calculation of X_G is possible if all these parameters are available, particularly in the MAGIC framework where we have access, along with all the instruments involved, to the balloons and radiosondes data (temperature, surface pressure, relative humidity, etc…). Thus, for these particular campaigns, X_G values will be calculated for CHRIS using ARAHMIS, and the results will be compared with the other instruments involved, especially the IFS125HR of the TCCON network and the EM27/SUN, and this will be the subject of the upcoming paper. However, the two equations for the calculation of X_G are not strictly similar since the EM27/SUN eliminates the systematic errors that are common to the target gas and O_2 column retrievals which will not be possible for us, since the O_2 band is not detected by CHRIS.
In addition, the total column uncertainty is calculated by summing the concentration of each layer along the profile weighted by the column of dry air based on figures 8 and 9. Table 2 lists the propagated uncertainties of the total column for both SZA using a diagonal a priori covariance matrix: the uncertainty of CO_2 total column is 2.89% and 2.6% for 10° and 80° respectively; while the uncertainty for CH_4 total column is 4.4% and 4.19% for 10° and 80° respectively. The uncertainties are smaller for a SZA of 80°, because the information distribution is improved with a longer OPD. Furthermore, these results show that the total profile error for CH_4 is almost 2 times higher than that of CO_2, but this is explained by the fact that our profile error is limited by the a priori profile error which is much higher for CH_4 than for CO_2. The dominating component of the uncertainty comes from the smoothing and predominates the other uncertainties for both GHG and is the major contributor to the total profile error. H_2O, temperature and SZA are the most important parameters contributing to the forward model, which are represented by the non-retrieved parameters uncertainty. Additionally, it is important to note that there is a supplementary uncertainty associated to the spectroscopy unaccounted for in our study, which is purely systematic. It's not simple to evaluate

485 in this case, because we use different spectral domains each having different spectroscopic uncertainties listed in the HITRAN database.

Error	CO_2		CH_4	
SZA	10°	80°	10°	80°
Smoothing	2.79	2.51	4.34	4.11
Measurement	0.6	0.54	0.59	0.7
Non-retrieved parameters	0.14	0.12	0.27	0.5
Total	2.89	2.6	4.4	4.19

Table 2: The total column errors for CO_2 and CH_4 profiles for CHRIS for the two SZA. The uncertainties are shown in percentages (%).

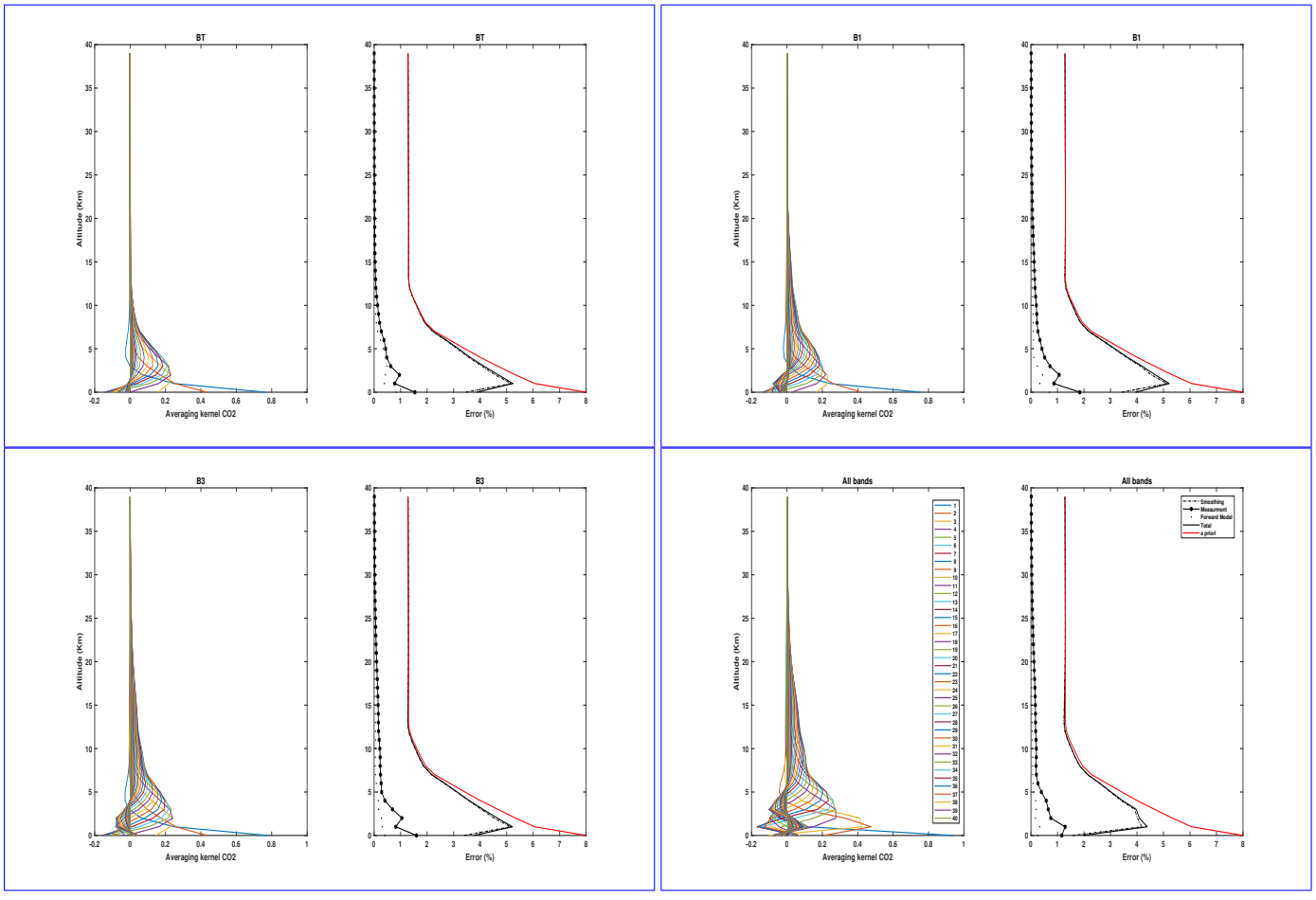

Fig. 8: Averaging kernels and error budgets of CO_2 vertical profiles for bands BT, B1 and B3 separately and all the bands together for an angle of 10° for CHRIS. The red and solid black lines stand for the prior (S_a) and posterior (S_x) errors respectively; the smoothing ($S_{smoothing}$), measurement ($S_{meas.}$), and forward model parameters ($S_{fwd.mod.}$) errors are dashed/dotted, dashed/starred and dotted, respectively.

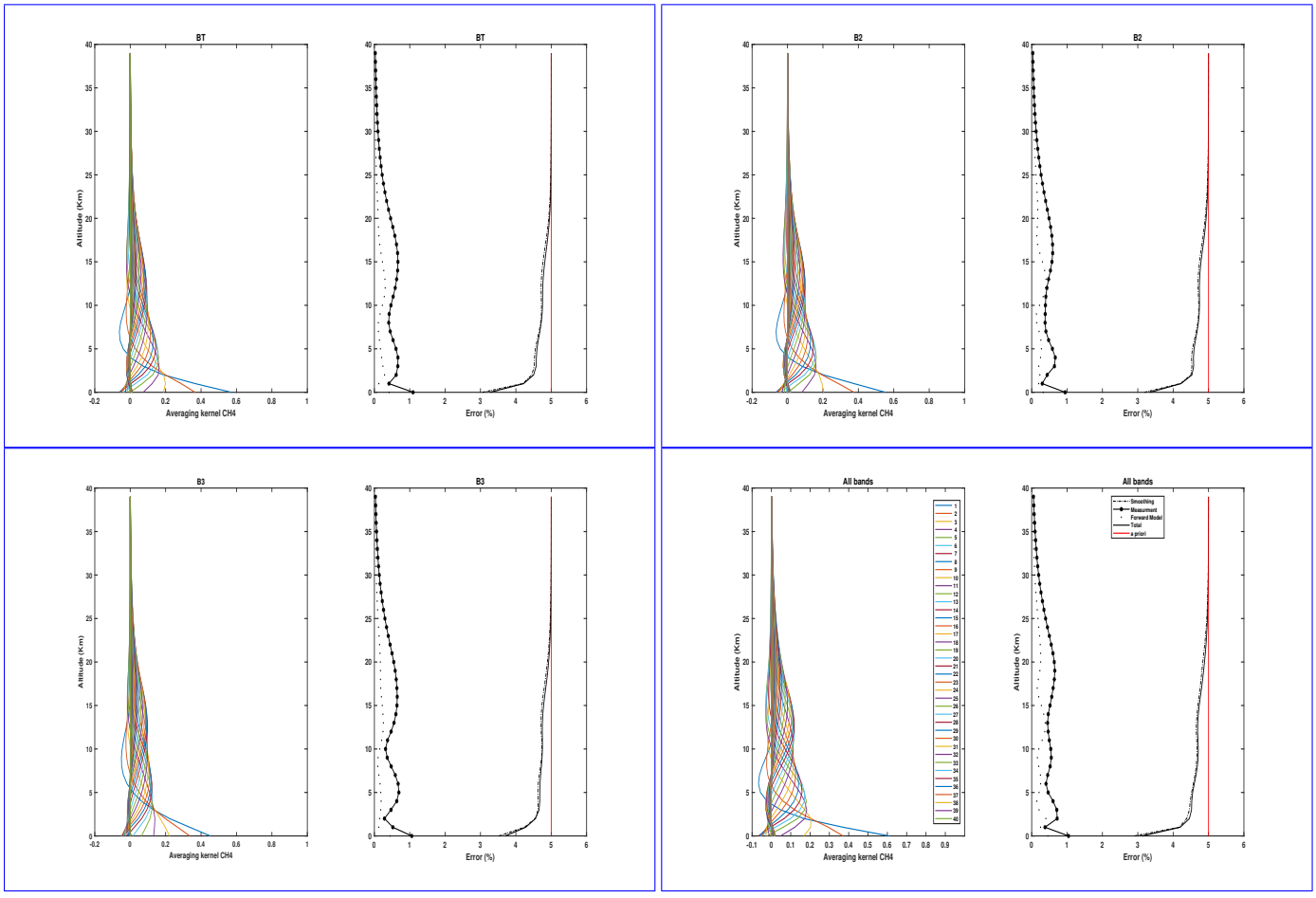

Fig. 9: Same as Fig. 8, but for CH_4 with bands BT, B2, B3 and all the bands together.

~~Averaging kernels and error budgets of CO_2 vertical profiles for bands BT, B1 and B3 separately and all the bands together for an angle of 10° for CHRIS. The red and solid black lines stand for the prior (S_a) and posterior (S_x) errors respectively; the smoothing ($S_{smoothing}$), measurement ($S_{meas.}$), and forward model parameters ($S_{fwd.mod.}$) errors are dashed/dotted, dashed/starred and dotted, respectively.~~

~~The CHRIS spectrometer with the attached tracker during one the 2018 MAGIC campaigns.~~

3.5 Comparison and complementary information content analysis for HR125, EM27/SUN and CHRIS

During the MAGIC campaigns, several ~~EM27-SUN and one~~ EM27/SUN and two IFS125HR from the TCCON network were operated alongside CHRIS~~showed in Fig. ??. An extensive~~ . An information content analysis is presented in the following sections for both of these instruments in order to compare and complement the study performed on CHRIS in Section 3.4.

3.5.1 Complementary information with ~~EM27-SUN~~EM27/SUN

In this section, an ~~extensive~~ IC study is ~~presented for the EM27-SUN~~ performed for the EM27/SUN instrument in order to compare it with our results and to investigate the possibility of complementing the data we obtained from CHRIS, especially for MAGIC. The bands of EM27/SUN used in this study are denoted as follows: B3, the common band with CHRIS, with a spectral range of 4700-5200 cm^{-1}, B4 going from 5460 cm^{-1} to 7200 cm^{-1}, and B5 spanning the spectral region between 7370 and 12500 cm^{-1}.

Firstly, ~~an information content study~~ a similar study to CHRIS is performed on ~~EM27-SUN~~ the EM27/SUN for CO_2 and CH_4 separately. As mentioned in Section 3.4, the state vector is constituted of only one of the gases concentrations with the same profile at a layer going from 0 to ~~20~~ 40 Km; however, we took into account the SNR and spectral resolution specific

	Resolution (cm^{-1})	MOPD (cm)	Spectral region (cm^{-1})	SNR
CHRIS	0.135	4.42	BT: 680-1250 B1: 1800-2300 B2: 2400-3600 B3: 3900-5200	780
EM27-SUN	0.5	1.8	B3: 4700-5200 B4: 5460-7200 B5: 7370-12500	1080
IFS125HR (TCCON) IFS125HR (NDACC)	~~5x10^{-3}~~ 0.02 0.0035-0.007	45 128-257	~~5-50000~~ 4000-15000 5-5200	~750 ~1000

Table 3: Instrumental characteristics of CHRIS, EM27-SUN and IFS125HR of both NDACC and TCCON.

to this instrument (see Table 3). Similar to the reasoning for CHRIS followed in Section 3.4, this study shows that using all the EM27/SUN bands together leads to an improvement of the a posteriori error profile on CO_2 concentrations, especially in the lower part of the atmosphere. Table 4 shows the DOFS for CO_2 of ~~EM27-SUN:~~ EM27/SUN: using a diagonal a priori covariance matrix for an angle of 10°, the total DOFS for bands B3 (common band with CHRIS), B4 and all bands together are: ~~2.98, 1.65 and 3.06 respectively, compared to 3.2, 2.36 and 3.34 for an angle of 80°~~2.95, 1.63 and 3.03 respectively. If only band B3 is taken into consideration which is the common band between the two instruments, the DOFS of CHRIS in this band is, as stated before, ~~3.12 and 3.46~~ 2.62 and 3.34 for an angle of 10° and 80° respectively, compared to ~~2.98 and 3.2~~ 2.95 and 3.17 for EM27/SUN. Therefore, the same number of partial columns can be retrieved using CHRIS (see Section 3.4) for CO_2 in this band. ~~However, an additional column can be retrieved using CHRIS if all the bands are used. Similar to the reasoning for CHRISfollowed in Section 3.4, this study shows that using all the EM27-SUN bands together leads to an improvement of the a posteriori error profile on CO_2 concentrations, especially in the lower part of the atmosphere~~Furthermore, similarly to CHRIS, while using a non-diagonal a priori covariance matrix (Eguchi et al. (2010)), the total error is reduced with a more propagated smoothing error on the profile and a reduction in the DOFS. As for CH_4 and referring to Table 3, band 3 in this instrument begins (4700 cm^{-1}) where the CH_4 band ends (4150-4700 cm^{-1}) in IFS125HR and CHRIS. This is important because TCCON networks ~~often~~ begin their measurements at 4000 cm^{-1} that allowed us the comparison with the band 3 of CHRIS (for both CO_2 and CH_4). However, the EM27/SUN have no exploitable signal before 4700 cm^{-1} ~~to coincide with the EM27-SUN and satellite data, therefore eliminating~~ (Gisi et al. (2012)), therefore the CH_4 ~~band from their spectra, this is why CHRIS and EM27-SUN have no common methane bands~~ absorption lines do not show in the common band between CHRIS and the EM27/SUN so the results ~~will not be~~ are not discussed here.

Secondly, a simultaneous IC study was performed on all the channels of both CHRIS and ~~EM27-SUN~~ EM27/SUN in order to analyze the complementary aspect of these two instruments. The results of this study are shown in Fig. 10. The DOFS obtained for CO_2 is ~~3.58 and 3.9~~ 3.67 and 3.93 for angles 10° and 80° respectively; and for CH_4 ~~3.87 and 4.29~~3.99 and 4.43. This indicates a ~~slight improvement in the retrieval~~ significant improvement of the retrieval when the spectral synergy TIR/SWIR/NIR is used, but less than the one obtained from space (for example TANSO-FTS in Herbin et al. (2013a))~~where the coupling TIR/SWIR, gives an advantage over the more pronounced difference MIR/SWIR between CHRIS and EM27-SUN. In addition, the computational time is very large, so the benefit of a simultaneous retrieval depends on the additional computing time generated.~~, since the measurement is obtained from the same optical path.

~~However, in the NIR, the error budget is performed by monitoring the observed O_2 columns where column-averaged dry-air mole fractions (denoted X_G for gas G) is calculated by rationing the gas retrieved slant column to the O_2 retrieved slant column for the same spectrum, which allows the reduction of a major part of the bias and the systematic errors during the measurement and its inversion process.The calculation of X_G will allow the EM27-SUN community to compare their results with the satellites data. This is not possible for CHRIS because it covers the MIR region where the O_2 molecule is missing in the spectra.~~

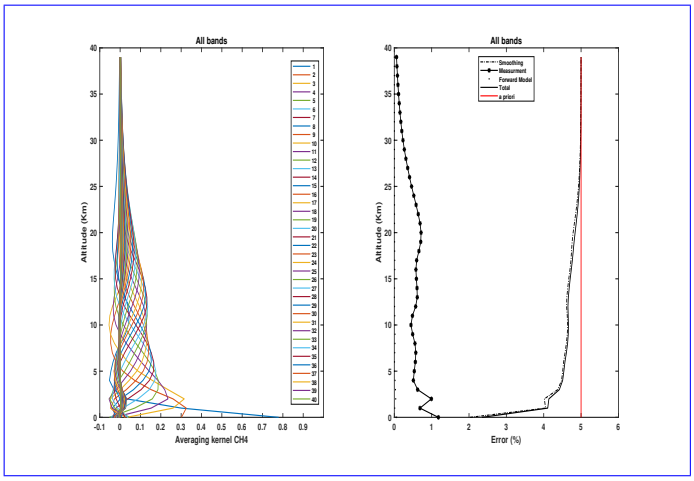

Fig. 10: Averaging kernels and error budgets of CO_2 and CH_4 vertical profiles for all the bands together for EM27/SUN and CHRIS combined for an angle of 10°. The red and black lines stand for the prior (S_a) and posterior (S_x) errors respectively; the smoothing ($S_{smoothing}$), measurement ($S_{meas.}$), and forward model parameters ($S_{fwd.mod.}$) errors are dashed/dotted, dashed/starred and dotted, respectively.

		BT	B1	B3	B4	All bands	
		DOFS				DOFS	Error
CHRIS	Angle 10	~~2.56~~ 2.01	~~2.42~~ 2.32	~~3.12~~ 2.62	-	~~3.52~~ 2.95	~~2.62~~2.89%
	Angle 80	2.56	2.67	3.34	-	3.71	2.6%
CHRIS with covariance	~~2.74~~ Angle 10	~~3.46~~ 1.45	1.7	2.15	-	~~3.79~~ 2.38	~~2.55~~1.01%
	Angle 80	1.89	1.92	2.68	-	3.08	0.94%
EM27/SUN	Angle 10	-	-	~~2.98~~ 2.95	~~1.65~~ 1.63	~~3.06~~ 3.03	~~2.74~~2.77%
	Angle 80	-	-	~~3.2~~ 3.17	~~2.36~~ 2.33	~~3.34~~ 3.31	~~2.64~~2.67%
EM27/SUN with covariance	Angle 10	-	-	2.25	1.17	2.37	1.01%
	Angle 80	-	-	2.53	1.71	2.68	0.97%
IFS125HR	Angle 10	~~2.89~~ 2.15	~~2.86~~ 2.33	~~3.72~~ 3.07	~~2.73~~ 2.62	~~4.32~~ 3.9	~~2.54~~2.82%
	Angle 80	~~2.91~~ 2.51	~~3.25~~ 2.61	~~4.07~~ 3.59	~~3.22~~ 2.99	~~4.56~~ 4.23	~~2.48~~2.72%
IFS125HR with covariance	Angle 10	1.66	1.85	2.86	2.3	3.28	0.97%
	Angle 80	1.97	2.14	3.04	2.61	3.53	0.95%

Table 4: The DOFS and column errors (%) of CO_2 for each band and for each instrument.

		BT	B2	B3	B4	All bands	
		DOFS				DOFS	Error
CHRIS	Angle 10	~~3.16~~ 2.77	~~3.55~~ 2.87	~~2.82~~ 2.62	-	~~3.86~~ 3.34	~~4.22~~4.4%
	Angle 80	~~3.28~~ 3.19	~~3.95~~ 3.88	~~3.53~~ 3.45	-	~~4.27~~ 4.26	~~4.13~~4.19%
CHRIS with covariance	Angle 10	2.03	2.22	1.97	-	2.57	1.5%
	Angle 80	2.23	2.83	2.56	-	3.21	1.46%
EM27/SUN	Angle 10	-	-	-	~~1.73~~1.69	~~1.73~~ 1.69	4.67%
	Angle 80	-	-	-	~~2.47~~ 2.45	~~2.47~~ 2.45	~~4.51~~4.54%
EM27/SUN with covariance	Angle 10	-	-	-	1.18	1.18	1.59%
	Angle 80	-	-	-	1.81	1.81	1.55%
IFS125HR	Angle 10	~~3.93~~ 3.37	~~4.51~~ 3.97	~~3.87~~ 3.69	~~2.69~~ 2.56	~~4.88~~ 4.64	~~4.09~~4.23%
	Angle 80	~~4.11~~ 3.66	~~4.88~~ 4.42	~~4.41~~ 4.23	~~3.51~~ 3.35	~~5.27~~ 4.98	~~3.98~~4.21%
IFS125HR with covariance	Angle 10	2.45	3.03	2.79	1.83	3.55	1.47%
	Angle 80	2.57	3.34	3.22	2.45	3.81	1.46%

Table 5: The DOFS and column errors (%) of CH_4 for each band and for each instrument.

3.5.2 Comparison with IFS125HR

As mentioned before, IFS125HR is a ground-based high resolution infrared spectrometer ~~installed in many of the NDACC stations, and some TCCON stations with a SNR of the order of 1000 (Schneider and Hase (2008))~~used in the NDACC and TCCON stations across the world. We performed ~~an~~ a similar information content study ~~on this instrument to compare it with our results~~ only on the TCCON instrument since this network is involved in the MAGIC campaigns therefore the results can be compared. For simplicity, the same annotation of the bands is kept for this section. The same methodology described in Section 3.4 is used here: the state vector is constituted of only CO_2 and CH_4 concentrations at a layer going from 0 to ~~20~~ 40 km where the SNR and the spectral resolution specific to the IFS125HR ~~instrument~~ are taken into consideration (see Table 3). We follow the same reasoning as the sections before: ~~the DOFS of CO_2, as shown in Table 4, for an angle of 10° are: 2.89, 2.86, 3.72, 2.73 and 4.32 for BT, B1, B3, B4 and all bands respectively, compared to 2.91, 3.25, 4.07, 3.22 and 4.56 for an angle of 80°. However, the DOFS of CH_4 , as shown in Table 5, for an angle of 10° are: 3.93, 4.51, 3.87, 2.69 and 4.88 for BT, B2, B3, B4 and all bands respectively, compared to 4.11, 4.88, 4.41, 3.51 and 5.27 for an angle of 80°. On the one hand, one additional partial tropospheric column for CO_2 can be retrieved with respect to: CHRIS for an angle of 80°, and EM27-SUN for both angles, if all the bands are used. We obtain the same result for CH_4, one additional partial tropospheric column can be retrieved with respect to CHRIS, if B3 or all the bands are used and for both angles. However, three additional partial tropospheric columns can be retrieved with respect to the EM27-SUN instrument.Figure~~ Fig. 11 shows the averaging kernel A and the total posterior error S_x for CO_2 and CH_4, for an angle of 10°. ~~As a first look, we~~ We can see that the vertical distribution is more homogeneous than CHRIS and ~~EM27-SUN~~ EM27/SUN suggesting a high sensitivity at high altitudes although in the lower atmosphere, the a posteriori error S_x is significantly reduced. This is also shown in the error budget study: we can still distinguish the a posteriori total error (solid black line) from the a priori error (red line) even in the higher atmosphere. This is explained by the fact that the IFS125HR has a spectral resolution ~~30 times higher than CHRIS and 100 times higher than EM27-SUN~~higher than both CHRIS and EM27/SUN, so the measurement ~~will always improve~~ always improves our knowledge of the profile all along the atmospheric column. ~~This result, along with the one discussed in Section 3.5.1, shows that CHRIS is more efficient than the EM27-SUN and less efficient than the IFS125HR in terms of the retrieval of GHG measurements.~~ Also, when using a non-diagonal a priori covariance matrix, the total profile error is significantly reduced, especially for CH_4, however, the DOFS is also reduced.

The DOFS of CO_2 and CH_4, as shown in Table 4, for both viewing angles and a priori covariance matrices. On the one hand, one additional partial tropospheric column for CO_2 can be retrieved with respect to CHRIS for an angle of 10°, and EM27/SUN for both angles, if all the bands are used. On the other hand, one additional partial tropospheric column can be retrieved for CH_4 with respect to CHRIS, if all the bands are used and for both angles.

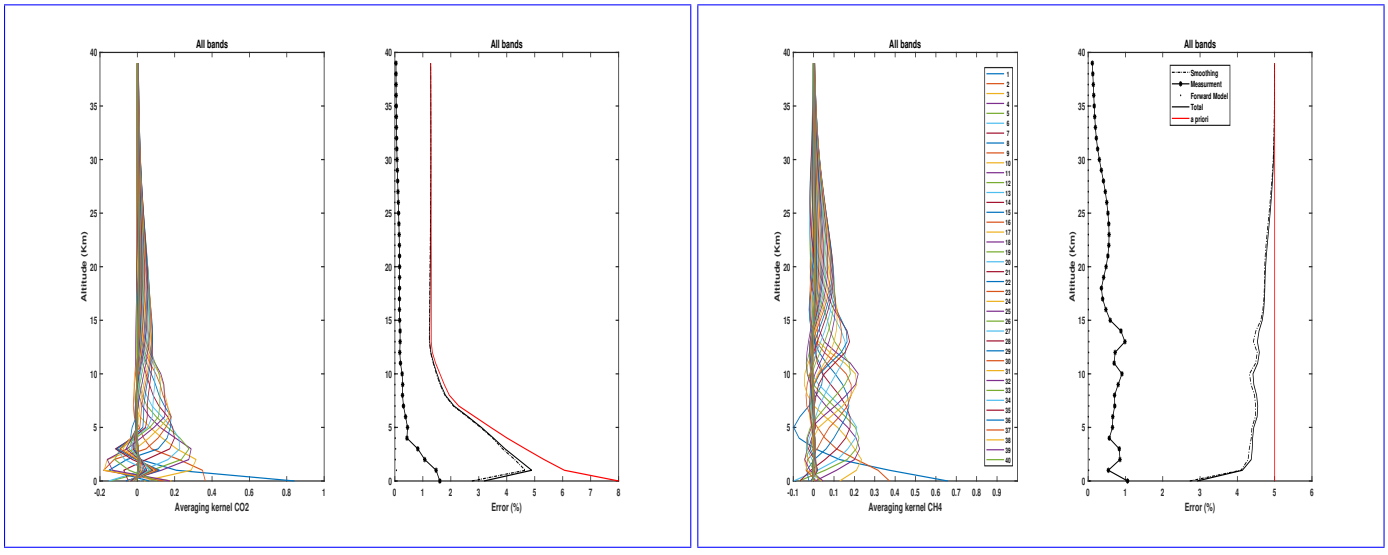

Fig. 11: Averaging kernels and error budgets of CO_2 and CH_4 and vertical profiles for bands all the bands together for an angle of 10° for IFS125HR. The red and black lines stand for the prior (S_a) and posterior (S_x) errors respectively; the smoothing ($S_{smoothing}$), measurement ($S_{meas.}$), and forward model parameters ($S_{fwd.mod.}$) errors are dashed/dotted, dashed/starred and dotted, respectively.

	CO_2		CH_4	
DOFS	90%	99%	90%	99%
Number of channels	1329	4648	1387	5924
% of the total number of channels	2.15%	7.54%	2.25%	9.61%

Table 6: Corresponding number of selected channels for the DOFS of CO_2 and CH_4 and their respective percentage of the total number of channels for CHRIS.

4 Channel selection

Using all the channels ~~, measured by CHRIS,~~ in the retrieval ~~scheme~~ process has two disadvantages. First of all, it requires a very large computational time. Secondly, the correlation of the interfering species increases the systematic error. In this case, the a priori state vector x_a and the error covariance matrix S_a is very difficult to evaluate. Channel selection is a method described by Rodgers (2000) to optimize a retrieval by objectively selecting the subset of channels that provides the greatest amount of information from high-resolution infrared sounders. L'Ecuyer et al. (2006) offers a description of this procedure based on the Shannon information content. ~~This approach is based on a sequential modification of the covariance matrix that will reduce the amount of time needed to perform the numerous matrix operations necessary for repeated application of the previous equations.~~ Firstly, we create ~~what we call~~ an "information spectrum" in order to evaluate the information content with respect to the a priori state vector. The channel with the largest amount of information is then selected. A new spectrum is then calculated with a new ~~posterior~~ posteriori covariance matrix that is adjusted according to the channel selected on the first iteration to account for the information it provides. In this way a second channel is chosen, based on this newly defined state space, that provides maximal information relative to the new a ~~posterior~~ posteriori covariance matrix. This process is repeated and channels are selected sequentially until the information in all the remaining channels falls below the level of measurement noise. As stated by Shannon information content and noted in Rodgers (2000), it is convenient to work in a basis where the measurement errors and prior variances are uncorrelated in order to compare the measurement error with the natural variability of the measurements across the full prior state. Therefore, it is desirable to transform the Jacobian matrix K (see Sect. 3.2) into $\widetilde{K}$ using:

$$\widetilde{K} = S_y^{-1/2} K S_a^{1/2} \tag{16}$$

which offers the added benefit of being the basis where both the a priori and the measurement covariance matrices are unit matrices. Furthermore, Rodgers demonstrates that the number of singular values of $\widetilde{K}$ greater than unity defines the number of independent measurements that exceed the measurement noise defining the effective rank of the problem.
Letting S_i be the error covariance matrix for the state space after i channels have been selected, the information content of channel j of the remaining unselected channels is given by:

$$H_j = \frac{1}{2} log_2(1 + \widetilde{k}_j^T S_i \widetilde{k}_j), \tag{17}$$

where $\widetilde{k}_j$ is the jth row of $\widetilde{K}$. H_j constitutes the information spectrum from which the first channel is selected. Taking the chosen channel to be channel l, the covariance matrix is then updated before the next iteration using the following statement:

$$S_{i+1}^{-1} = S_i^{-1} + \widetilde{k}_l \widetilde{k}_l^T \tag{18}$$

In this way, channels are selected until 90% of the total information spectrum H is reached in a way that the measurement noise is not exceeded.
After that, H expressed in bits is converted to DOFS to obtain Fig. 12 that represents the CO_2 and CH_4 total DOFS evolution as a function of the number of selected channels and ~~from~~ for all spectral bands and for a SZA of 10°. CHRIS has 75424 channels in total, 13800 are unusable because of the water vapor saturation between the bands, which leaves us with 61624 exploitable channels. A pre-selection of these channels, based on Fig.7, is done where the number of exploitable channels is reduced to the spectral areas where we find CO_2 and CH_4 (13447 and 19751 pre-selected channels respectively). At a first look at Figure 12, the DOFS for each gas increases sharply with the first selected channels and then more steadily. The number of channels required to reach 90% and 99% of the total information ~~provided by using all the channels~~ is represented in Table 6. For CO_2, out of the 1329 channels, 55.76% of the information comes from B3 (common band with the EM27/SUN), 37.24% from BT and 6.99% from B1. As for CH_4, out of the 1387 channels, 46.86% of the information comes from B2, 28.19% from BT and 24.9% from B3. This result shows that most of the information for CO_2 and CH_4 comes from ~~band 3 (~~B3 ~~) and the thermal band (BT)~~ and BT respectively, which indicates that the synergy between TIR and SWIR observations is confirmed.
Furthermore, the 1329 and 1387 selected channels represent 2.15% and 2.25% of the 61624 exploitable channels respectively, so a retrieval ~~scheme~~ process that uses selected channels corresponding to 90% of the total information content would give comparable ~~errors~~ results to the one using the entire set of channels since almost 98% of the information is redundant. Hence, these results indicate the interest of determining an optimal set of channels for each gas separately, ~~so the inversion process will be~~ this is why this channel selection will be used in the retrieval process making it easier and less time consuming.

5 Conclusions

~~To summarize, the work done in this paper ,~~ In conclusion, this paper presents the characteristics of ~~a~~ the new infrared spectrometer ~~called~~ CHRIS that allows the retrieval of GHG and trace gases. This instrumental prototype has unique characteristics, such as its high spectral resolution (0.135 cm^{-1}) and wide spectral range (680-5200 cm^{-1}) covering the MIR region. In the context of its exploitation ~~in field campaigns, especially MAGIC,~~ to retrieve GHG, ~~we calibrated this instrument spectrally and radiometrically as well as performed~~ spectral and radiometric calibrations were performed using a calibrated external blackbody reaching a temperature of 1523 K. Additionally, between laboratory calibrations and during field campaigns the radiometric stability is monitored through measurements of the internal blackbody. In the MAGIC framework, an extensive information content analysis ~~. A comparison and a complementary study was made,~~ is performed showing the potential capabilities of this instrument to retrieve GHG, using two different SZA (10° and 80°) to quantify the improvement of the information with the solar optical path. Furthermore, two a priori covariance matrices were used: one diagonal and another derived from climatological data. The total column uncertainty is estimated showing that when using a diagonal a priori covariance matrix the error for an angle of 10° is of the order of 2.89% for CO_2 and 4.4% for CH_4 for all the bands; however, when using a climatological distribution the total column error for the same angle and for all the bands is reduced to 1.01% for CO_2 and 1.5% for CH_4 but with a significant decrease in the DOFS (from 2.95 to 2.38 for ~~two commercial ground-based instruments, one of them being part of the TCCONnetwork. The~~ CO_2 and from 3.34 to 2.57 for CH_4). Also, a comparison study with the IFS125HR of the TCCON, which is widely used in the satellite validation process, is performed illustrating the benefits of its high spectral resolution on GHG retrievals. Moreover, a complementary study is carried out on the EM27/SUN to investigate the possibility of a retrieval exploiting the synergy between TIR~~and SWIRobservations was also discussed. Future work will focus on the retrieval of tropospheric columns and the inversion process of the GHG,~~ /SWIR/NIR observations, which showed

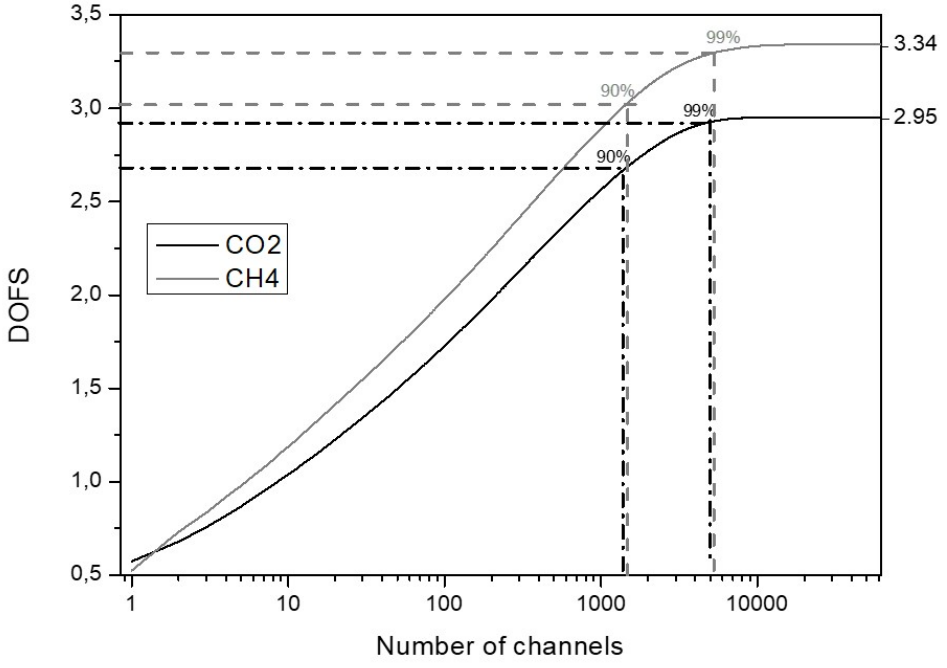

Fig. 12: Evolution of the ~~DOFSs~~ DOFS with the number of selected channels for CO_2 (~~red line~~black) and CH_4 (~~green line~~gray).

that a significant improvement can be obtained, for example with a SZA of 10° the DOFS is increased from 2.95 to 3.67. Finally, a channel selection is implemented to remove the redundant information. The latter will be used in the future work dedicated to the CO_2 and CH_4 ~~, using the line-by-line radiative transfer algorithm ARAHMIS and the validation of our results with the MAGIC campaign data~~total columns retrievals for the MAGIC campaigns.

Acknowledgements. The CaPPA project (Chemical and Physical Properties of the Atmosphere) is funded by the French National Research Agency (ANR) through the PIA (Programme d'Investissement d'Avenir) under contract "ANR-11-LABX-0005-01" and by the Regional Council "Nord Pas de Calais-Picardie" and the "European Funds for Regional Economic Development" (FEDER). Financial support from CNES TOSCA (MAGIC) is also acknowledged.
Also we acknowledge the "Ecole centrale de ~~lille~~Lille" for its help in providing the cavity blackbody used in the calibration process. ~~IT support from Fabrice Ducos is also acknowledged~~We express our appreciation for the Pr. Denis Petiprez for his help with the determination of the ILS. Finally, we are also immensely grateful to Fabrice Ducos who provided technical expertise that greatly assisted the research and for his work on ARAHMIS.

References

Aumann, H. H., Chahine, M. T., Gautier, C., Goldberg, M. D., Kalnay, E., McMillin L. M., Revercomb, H., Rosenkranz, P. W., Smith, W. L., Staelin, D. H., Strow, L. L., and Susskind, J.: *AIRS/AMSU/HSB on the Aqua mission: design, science objectives, data products, and processing systems*, IEEE Trans. Geosci. Remote Sens., 41, 253-264, https://doi.org/10.1109/TGRS.2002.808356, 2003.

Clarisse, L., Hurtmans, D., Prata, A. J., Karagulian, F., Clerbaux, C., Mazière, M. D., and Coheur, P.-F.: Retrieving radius, concentration, optical depth, and mass of different types of aerosols from high-resolution infrared nadir spectra, Appl. Opt., 49, 3713-3722, 10.1364/AO.49.003713, 2010.

Clerbaux, C., Hadji-Lazaro, J., Turquety, S., George, M., Coheur, P.-F., Hurtmans, D., Wespes, C., Herbin, H., Blumstein, D., Tourniers, B., and Phulpin, T.: The IASI/MetOp1 Mission: First observations and highlights of its potential contribution to GMES2, Space Res. Today, 168, 19-24, https://doi.org/10.1016/S0045-8732(07)80046-5, 2007.

Clough, S. A., Shephard, M. W., Mlawer, E. J., Delamere, J. S., Iacono, M. J., Cady-Pereira, K., Boukabara, S., and Brown, P.D.: Atmospheric radiative transfer modeling: a summary of the AER codes, JQSRT, 91, 233-244, 10.1016/j.jqsrt.2004.05.058, 2005.

De Wachter, E., Kumps, N., Vandaele, A. C., Langerock, B., and De Mazière, M.: Retrieval and validation of MetOp/IASI methane, Atmos. Meas. Tech., 10, 4623–4638, https://doi.org/10.5194/amt-10-4623-2017, 2017.

Dohe, S., Sherlock, V., Hase, F., Gisi, M., Robinson, J., Sepúlveda, E., Schneider, M., and Blumenstock, T.: A method to correct sampling ghosts in historic near-infrared Fourier transform spectrometer (FTS) measurements, Atmos. Meas. Tech., 6, 1981–1992, https://doi.org/10.5194/amt-6-1981-2013, 2013.

Eguchi, N., Saito, R., Saeki, T., Nakatsuka, Y., Belikov, D., and Maksyutov, S. (2010), A priori covariance estimation for CO2 and CH4 retrievals, J. Geophys. Res., 115, D10215, doi:10.1029/2009JD013269.

Gisi, M., Hase, F., Dohe, S., Blumenstock, T., Simon, A., and Keens, A.: XCO_2-measurements with a tabletop FTS using solar absorption spectroscopy, Atmos. Meas. Tech., 5, 2969-2980, https://doi.org/10.5194/amt-5-2969-2012, 2012.

Gordon, I. E., Rothman, L. S., Hill, C., Kochanov, R. V., Tan, Y., Bernath, P. F., Birk, M., Boudon, V., Campargue, A., Chance, K., Drouin, B. J., Flaud, J.-M., Gamache, R. R., Hodges, J. T., Jacquemart, D., Perevalov, V. I., Perrin, A., Shine, K. P., Smith, M.-A. H., Tennyson, J., Toon, G. C., Tran, H., Tyuterev, V. G., Barbe, A., Császár, A. G., Devi, V. M., Furtenbacher, T., Harrison, J. J., Hartmann, J.-M., Jolly, A., Johnson, T. J., Karman, T., Kleiner, I., Kyuberis, A. A., Loos, J., Lyulin, O. M., Massie, S. T., Mikhailenko, S. N., Moazzen-Ahmadi, N., Muller, H. S. P., Naumenko, O. V., Nikitin, A. V., Polyansky, O. L., Rey, M., Rotger, M., Sharpe, S. W., Sung, K., Starikova, E., Tashkun, S. A., Auwera, J. V., Wagner, G., Wilzewski, J., Wcislo, P., Yu, S., and Zak, E.J.: The HITRAN2016 molecular spectroscopic database, J. Quant. Spectrosc. Radiat. Transf., 203, 3-69, https://doi.org/10.1016/j.jqsrt.2017.06.038, 2017.

Herbin, H., Labonnote, L. C., and Dubuisson, P.: Multispectral information from TANSO-FTS instrument – Part 1: Application to greenhouse gases (CO_2 and CH_4) in clear sky conditions, Atmos. Meas. Tech., 6, 3301–3311, https://doi.org/10.5194/amt-6-3301-2013, 2013.

Kobayashi, N., Inoue, G., Kawasaki, M., Yoshioka, H., Minomura, M., Murata, I., Nagahama, T., Matsumi, Y., Tanaka, T., Morino, I., and Ibuki, T.: Remotely operable compact instruments for measuring atmospheric CO_2 and CH_4 column densities at surface monitoring sites, Atmos. Meas. Tech., 3, 1103–1112, https://doi.org/10.5194/amt-3-1103-2010, 2010.

L'Ecuyer, T. S., Gabriel, P., Leesman, K., Cooper, S. J., Stephens, G. L.: Objective Assessment of the Information Content of Visible and Infrared Radiance Measurements for Cloud Microphysical Property Retrievals over the Global Oceans. Part I: Liquid Clouds, J. Appl. Meteorol. Clim., 45, 20-41, https://doi.org/10.1175/JAM2326.1, 2006.

Michalsky, J. J.: The Astronomical Almanac's algorithm for approximate solar position (1950–2050), J. Sol. Energy, 40, 227-235, https://doi.org/10.1016/0038-092X(88)90045-X, 1988.

Pathakoti, M., Gaddamidi, S., Gharai, B., Mullapudi Venkata Rama, S. S., Kumar Sundaran, R., and Wang, W.: Retrieval of CO_2, CH_4, CO and N_2O using ground- based FTIR data and validation against satellite observations over the Shadnagar, India, Atmos. Meas. Tech. Discuss., https://doi.org/10.5194/amt-2019-7, 2019.

Persky, M. J.: A review of spaceborne infrared Fourier transform spectrometers for remote sensing, Rev. Sci. Instrum., 66, 4763-4797, https://doi.org/10.1063/1.1146154, 1995.

Petri, C., Warneke, T., Jones, N., Ridder, T., Messerschmidt, J., Weinzierl, T., Geibel, M., and Notholt, J.: Remote sensing of CO_2 and CH_4 using solar absorption spectrometry with a low resolution spectrometer, Atmos. Meas. Tech., 5, 1627–1635, https://doi.org/10.5194/amt-5-1627-2012, 2012.

Razavi, A., Clerbaux, C., Wespes, C., Clarisse, L., Hurtmans, D., Payan, S., Camy-Peyret, C., and Coheur, P. F.: Characterization of methane retrievals from the IASI space-borne sounder, Atmos. Chem. Phys., 9, 7889-7899, https://doi.org/10.5194/acp-9-7889-2009, 2009.

Revercomb, H. E., Buijs, H., Howell, H. B., LaPorte, D. D., Smith, W. L., and Sromovsky, L. A.: Radiometric calibration of IR Fourier transform spectrometers: solution to a problem with the High-Resolution Interferometer Sounder, Appl. Opt., 27, 3210-3218, https://doi.org/10.1364/AO.27.003210, 1988.

Rodgers, C. D.: Inverse methods for atmospheric sounding : theory and practice, World Scientific Publishing, 2000.

Schmidt, U., and Khedim, A.: In situ measurements of carbon dioxide in the winter Arctic vortex and at midlatitudes : an indicator of the age of stratopheric air, Geophys. Res. Lett., 18, 763-766, https://doi.org/10.1029/91GL00022, 1991.

Schneider, M. and Hase, F.: Technical Note: Recipe for monitoring of total ozone with a precision of around 1 DU applying mid-infrared solar absorption spectra, Atmos. Chem. Phys., 8, 63-71, https://doi.org/10.5194/acp-8-63-2008, 2008.

Suto, H., Kuze, A., Kaneko, Y., and Hamazaki, T.: Characterization of TANSO-FTS on GOSAT, AGU Fall Meeting Abstracts, 2006.

Toon, G. C., Solar Line List for the TCCON 2014 Data Release, CaltechDATA, https://doi.org/10.14291/tccon.ggg2014.solar.r0/1221658, 2015.

Trishchenko, A. P.: Solar Irradiance and Effective Brightness Temperature for SWIR Channels of AVHRR/NOAA and GOES Imagers, J. Atmospheric Ocean. Technol., 23, 198-210, https://doi.org/10.1175/JTECH1850.1, 2006.

Wiacek, A., Taylor, J. R., Strong, K., Saari, R., Kerzenmacher, T. E., Jones, N. B., and Griffith, D. W. T.: Ground-Based Solar Absorption FTIR Spectroscopy: Characterization of Retrievals and First Results from a Novel Optical Design Instrument at a New NDACC Complementary Station, Jtech, 24, 432-448, 10.1175/JTECH1962.1, 2007.

Wunch, D., Toon, G. C., Blavier, J.-F. L., Washenfelder, R. A., Notholt, J., Connor, B. J., Griffith, D. W. T., Sherlock, V., and Wennberg, P. O.: The Total Carbon Column Observing Network, Philos. Trans. Royal Soc. A, 369, 2087-2112, https://doi.org/10.1098/rsta.2010.0240, 2011.

Zhou, M., Langerock, B., Sha, M. K., Kumps, N., Hermans, C., Petri, C., Warneke, T., Chen, H., Metzger, J.-M., Kivi, R., Heikkinen, P., Ramonet, M., and De Mazière, M.: Retrieval of atmospheric CH_4 vertical information from ground-based FTS near-infrared spectra, Atmos. Meas. Tech., 12, 6125–6141, https://doi.org/10.5194/amt-12-6125-2019, 2019.